Inorganic Chemistry

Article

pubs.acs.org/IC

Phosphorescent Platinum(II) Complexes Bearing 2-Vinylpyridine-type Ligands: Synthesis, Electrochemical and Photophysical Properties, and Tuning of Electrophosphorescent Behavior by Main-Group Moieties

Xiaolong Yang, Xianbin Xu, Jiang Zhao, Jing-shuang Dang, Zuan Huang, Xiaogang Yan, Guijiang Zhou,* and Dongdong Wang*

MOE Key Laboratory for Nonequilibrium Synthesis and Modulation of Condensed Matter, State Key Laboratory for Mechanical Behavior of Materials, and Institute of Chemistry for New Energy Materials, Department of Chemistry, Faculty of Science, Xi'an Jiaotong University, Xi'an 710049, P. R. China

Supporting Information

ABSTRACT: A series of 2-vinylpyridine-type platinum(II) complexes bearing different main-group blocks ($B(Mes)_2$, $SiPh_3$, $GePh_3$, NPh_2, $POPh_2$, OPh, SPh, and SO_2Ph, where Mes = 2-morpholinoethanesulfonic acid) were successfully prepared. As indicated by the X-ray single-crystal diffraction, the concerned phosphorescent platinum(II) complexes exhibit distinct molecular packing patterns in the solid state to bring forth different interactions between individual molecules. The photophysical characterizations showed that the emission maxima together with phosphorescent quantum yield of these complexes can also be affected by introducing distinct main-group moieties with electron-donating or electron-withdrawing characters. Furthermore, these 2-vinylpyridine-type platinum(II) complexes exhibit markedly different photophysical and electrochemical properties compared with their 2-phenylpyridine-type analogues, such as higher-lying highest occupied molecular orbital levels and lower-energy phosphorescent emissions. Importantly, these complexes can show good potential as deep red phosphorescent emitters to bring attractive electroluminescent performances with Commission Internationale de L'Eclairage (CIE) coordinates very close to the standard red CIE coordinates of (0.67, 0.33) recommended by the National Television Standards Committee. Hence, these results successfully established structure−property relationship concerning photophysics, electrochemistry, and electroluminescence, which will not only provide important information about the optoelectronic features of these novel complexes but also give valuable clues for developing novel platinum(II) phosphorescent complexes.

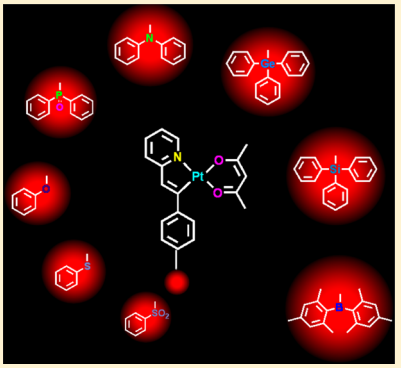

INTRODUCTION

Platinum(II) complexes, which are versatile materials, have been drawing substantial research enthusiasm because they can be used in several fields, including highly efficient organic light-emitting diodes (OLEDs) for display and solid-state lighting technologies,[1−5] solar energy conversion,[6−9] impressive optical power limiting materials,[10−13] and highly selective and sensitive chemical sensors.[14−16] Because of the high spin−orbit coupling (SOC) constant associated with the platinum atom, the triplet states (T_1) are preferentially generated through the efficient intersystem crossing (ISC) process in the platinum(II) complexes. The unique characters of T_1 states thus have successfully guaranteed the rich variety of properties of the platinum(II) complexes. The highly emissive T_1 states can be harnessed to improve the electroluminescence (EL) efficiencies of OLEDs dramatically.[17,18] The triplet excitons generated in platinum(II) complexes with high quantum yield (Φ) and long lifetime can facilitate the intermolecular charge-transport process, which is helpful to improve the output current of heterojunction organic photovoltaic (OPV) cells.[9] In addition, the efficient ISC processes in platinum(II) complexes will arouse intense triplet-state absorption, resulting in superb susceptibility of optical power limiting effect.[12] In general, the triplet states of the platinum(II) complexes are also extremely sensitive to oxygen due to the triplet−triplet annihilation caused by triplet ground state of oxygen.[19] Therefore, some suitable platinum(II) complexes have been used as highly selective and sensitive oxygen sensors.[20,21]

Clearly, the critical applications aforementioned associated with platinum(II) complexes are derived from T_1 states, whose different characters are afforded by the organic ligands with different structures. Hence, platinum(II) complexes with many kinds of organic ligands have been designed ingeniously, including porphyrin,[1,22,23] 2-phenylpyridine,[18,24,25] 1,3-bis(2-pyridyl)benzene,[26,27] 6-phenyl-2,2′-bipyridine,[28,29] and pyridyl azolate-based ligands[30,31] as well as their corresponding derivatives. In all of these traditional phosphorescent platinum-

Received: September 1, 2014
Published: December 4, 2014

   dx.doi.org/10.1021/ic502122t | Inorg. Chem. 2014, 53, 12986−13000

Scheme 1. Synthetic Route for 2-Vinylpyridine-type Platinum(II) Complexes

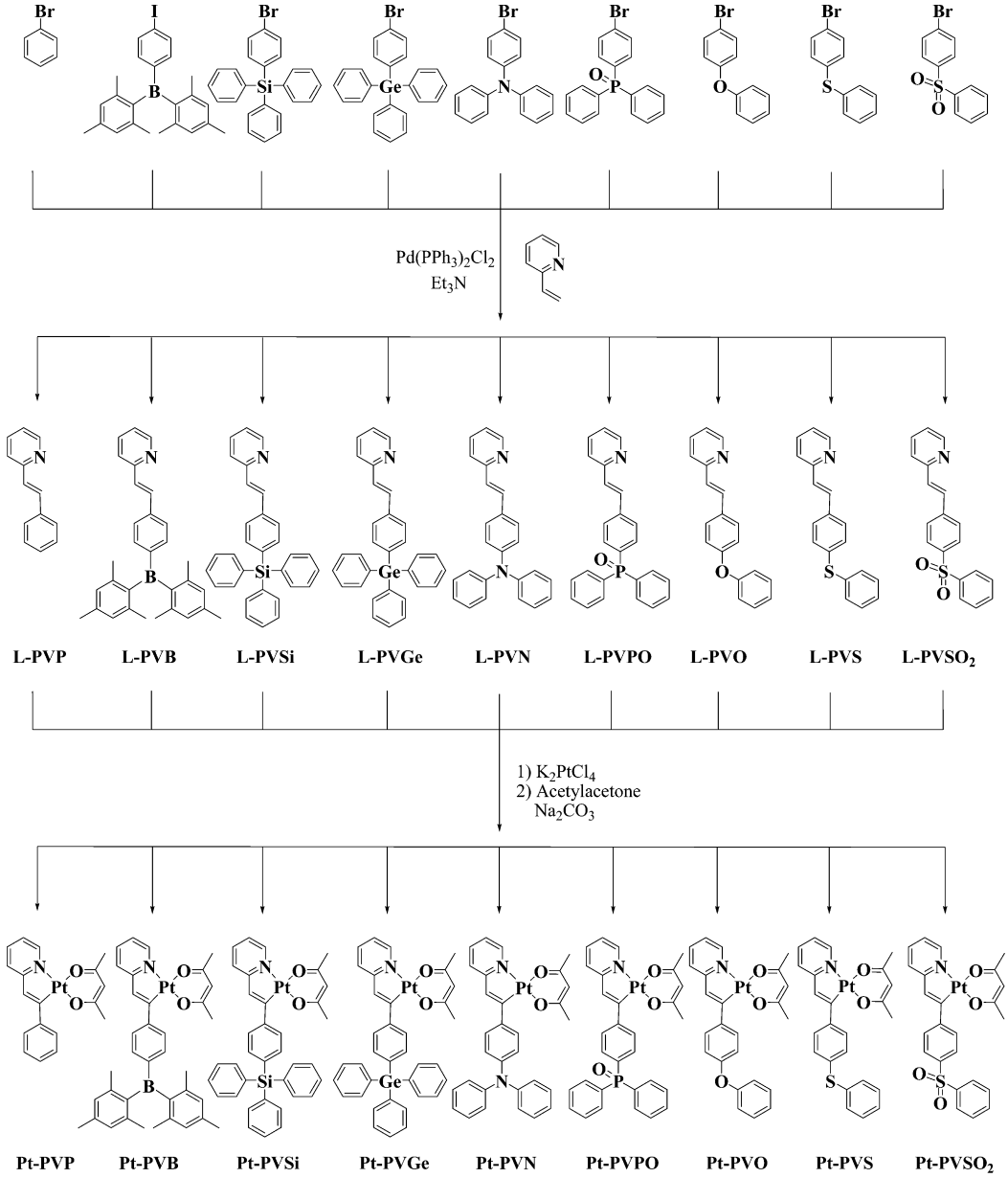

(II) complexes, the central Pt(II) ions are generally coordinated with the atoms in the aromatic system. This kind of coordinating pattern is quite conventional in the iridium(III) complexes as well.[32,33] However, novel phosphorescent iridium(III) complexes bearing 2-vinylpyridine-type ligands have also been developed as phosphorescent molecules. In these complexes, the Ir(III) metal center is chelated to the carbon atom in the vinyl group instead of to aromatic blocks.[34,35] Furthermore, the concerned phosphorescent iridium(III) complexes exhibit markedly different photophysical properties. However, to our best knowledge, there has been no report about the platinum(II) complexes bearing vinylpyridine-type ligands. Herein, with the aim to explore novel phosphorescent molecules, a series of platinum(II) complexes containing 2-vinylpyridine-type ligands was successfully conceived and prepared. Additionally, the structural features, electrochemical properties, and photophysical behaviors associated with these new complexes were carefully investigated. Through the concerned investigations, the relationship between the structural features of the platinum(II) complexes and their concerned properties was established, which should provide useful information for the design and synthesis of novel platinum(II) complexes.

RESULTS AND DISCUSSION

Synthesis and Characterizations. The synthetic detail of this series of platinum(II) complexes bearing 2-vinylpyridine-type ligands is shown in Scheme 1. With the aim to study the effect of the chemical structure of the organic ligands on the properties of these platinum(II) complexes and hence obtain the structure−property relationship, main-group moieties with distinct properties were introduced to the organic ligands. The synthetic procedures for the aryl halides with main-group units have been published elsewhere.[25,32] All the 2-vinylpyridine-type ligands were prepared by Heck coupling reaction between 2-vinylpyridine and the respective main-group functionalized aryl

dx.doi.org/10.1021/ic502122t | Inorg. Chem. 2014, 53, 12986−13000

Table 1. Crystal and Data Parameters for Structures Pt-PVSO$_2$, Pt-PVS, Pt-PVB, Pt-PVGe, and Pt-PVSi

compound	Pt-PVB	Pt-PVSi	Pt-PVGe	Pt-PVS	Pt-PVSO$_2$
CCDC No.	942 859	942 862	942 860	942 861	942 863
formula	$C_{36}H_{38}BNO_2Pt$	$C_{36}H_{31}NO_2PtSi$	$C_{36}H_{31}GeNO_2Pt$	$C_{24}H_{21}NO_2PtS$	$C_{24}H_{21}NO_4Pt$ S
formula weight	722.57	732.80	777.30	582.57	614.57
crystal system	triclinic	monoclinic	monoclinic	monoclinic	orthorhombic
space group	$P\bar{1}$	$P2(1)/c$	$P2(1)/c$	$P2(1)/c$	$P2(1)2(1)2(1)$
a (Å)	8.4647(8)	10.5375(8)	10.6036(8)	15.2526(11)	8.5632(6)
b (Å)	10.4529(9)	9.7960(8)	9.7918(7)	10.8566(8)	10.5141(8)
c (Å)	17.8442(15)	29.515(2)	29.608(2)	13.9408(10)	25.0136(18)
α (deg)	80.9970(10)	90	90	90	90
β (deg)	88.278(2)	93.348(2)	93.7450(10)	113.5590(10)	90
γ (deg)	85.0530(10)	90	90	90	90
V (Å^3)	1553.4(2)	3041.5(4)	3067.6(4)	2116.1(3)	2252.1(3)
Z	2	4	4	4	4
D_{calcd} (g cm^{-3})	1.545	1.600	1.683	1.829	1.813
crystal size (mm^3)	0.26 × 0.24 × 0.23	0.27 × 0.25 × 0.22	0.27 × 0.26 × 0.24	0.25 × 0.23 × 0.21	0.24 × 0.22 × 0.21
F(000)	720	1448	1520	1128	1192
μ (mm^{-1})	4.549	4.686	5.568	6.749	6.353
θ range (deg)	2.13−27.99	2.19−28.05	1.38−28.01	1.46−28.05	1.63−28.23
diffrn reflns number	9208	17 603	17 713	12 364	13 602
reflns number total	6674	6971	7047	4803	5409
no. of parameters	370	370	370	262	280
$R1$, $wR2$ $[I > 2.0\sigma\ (I)]$[a]	0.0386, 0.0834	0.0429, 0.0978	0.0370, 0.0670	0.0301, 0.0702	0.0603, 0.1516
$R1$, $wR2$ (all data)	0.0505, 0.0910	0.0772, 0.1153	0.0669, 0.0767	0.0469, 0.0891	0.0919, 0.1678
GOF on F^2 [b]	1.029	0.877	0.917	1.024	1.065

[a] $R1 = \Sigma||F_0| - |F_c||/\Sigma|F_0|$. $wR2 = \{\Sigma[w(F_0^2 - F_c^2)^2]/\Sigma\ [w(F_0^2)^2]\}^{1/2}$. [b] $\mathrm{GOF} = [(\Sigma w|F_0| - |F_c|)^2/(N_{obs} - N_{param})]^{1/2}$.

halides in the presence of triethylamine and $Pd(PPh_3)_2Cl_2$ with the yields ranging from 43.7% to 75.1%.[36] According to the previously reported methods,[18,25a] these platinum(II) complexes were obtained in two steps from K_2PtCl_4 and the corresponding ligands via Pt(II)-μ-chloro-bridged dimer as intermediate complexes. Purified by chromatography on silica columns, the 2-vinylpyridine-type platinum(II) complexes can be obtained in high purity. All complexes are air stable and were characterized by ^{1}H NMR and ^{13}C NMR. In the ^{1}H NMR spectra for all the platinum complexes, a single resonance peak around 6.50 ppm, which can be assigned to the proton on the vinyl unit, can be clearly seen, indicating the unique structural features of the complexes. To investigate the influence of different main groups on the properties of the concerned complexes, Pt-PVP is also obtained as the reference compound.

Single-Crystal X-ray Crystallography. The single crystals of Pt-PVSO$_2$, Pt-PVS, Pt-PVB, Pt-PVSi, and Pt-PVGe were successfully prepared by slow evaporation of their chloroform−hexane solutions. The structures of these complexes were determined by single-crystal X-ray crystallography. Details of each structure are given in Table 1.

Complexes Pt-PVSO$_2$ and Pt-PVS are chemically similar despite the sulfur atoms in Pt-PVSO$_2$ being in an oxidized state. As depicted in Figure 1, perspective views of Pt-PVSO$_2$ and Pt-PVS reveal that the platinum(II) ion is coordinated to N1 and C7 in the vinylpyridine moiety and two oxygen atoms from acetylacetone anion. The N1−Pt1−O2 angles in solid-state structures of Pt-PVSO$_2$ and Pt-PVS are 175.2(4)° and 176.04(16)° (Table 2), respectively, indicating that these platinum(II) complexes adopt a distorted square-planar geometry, which may result from the deviation of the vinylpyridine moiety from the ideal coplanar conformation. The Pt1−N1 distances in Pt-PVSO$_2$ (1.981(12) Å) and Pt-PVS (1.994(4) Å) are comparable to those in other ppy-type (Hppy = 2-phenylpyridine) platinum(II) complexes.[37] The Pt1−O1 (2.070(9) Å for Pt-PVSO$_2$, 2.081(4) Å for Pt-PVS) and Pt1−O2 (2.012(11) Å for Pt-PVSO$_2$, 2.001(4) Å for Pt-PVS) bond lengths are within the range of 1.985(6)−2.156(15) Å for other cyclometalated Pt(β-diketonato) complexes.[37,38] The bond length of Pt1−O1 *trans* to the C7 is significantly longer than that of Pt1−O2, indicating a stronger *trans* effect of vinyl carbon atom than that of the nitrogen donor atom.[39] The Pt−C bond length (1.977(13) Å for Pt-PVSO$_2$ and 1.987(5) Å for Pt-PVS) is longer than that in some ppy-type and lepidine-based platinum(II) complexes.[37,40] To our best knowledge, no literature has reported information about cyclometalated platinum(II) complexes containing vinylpyridine-type ligands, so these results might represent the first information about the structural parameters in this type of platinum(II) complex.

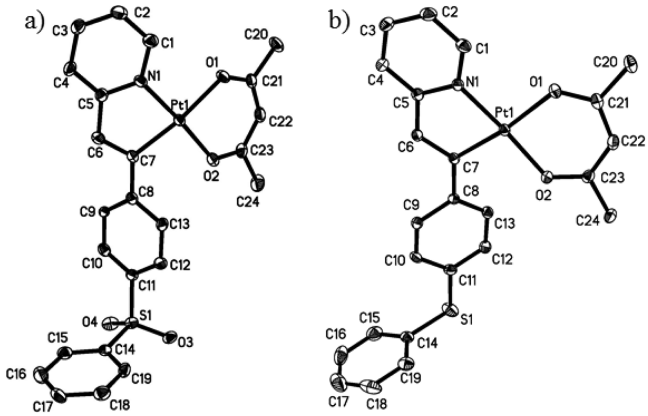

Figure 1. Perspective views of (a) Pt-PVSO$_2$ and (b) Pt-PVS. (All hydrogen atoms are omitted for clarity.) Thermal ellipsoids are drawn at the 15% probability level.

dx.doi.org/10.1021/ic502122t | Inorg. Chem. 2014, 53, 12986−13000

Table 2. Selected Crystallographic Data for Complexes Pt-PVSO$_2$, Pt-PVS, Pt-PVB, Pt-PVSi, and Pt-PVGe

bond lengths (Å) and angles (deg)			
Pt-PVSO$_2$			
Pt1−N1	1.981(12)	Pt1−C7	1.977(13)
Pt1−O1	2.070(9)	Pt1−O2	2.012(11)
N1−Pt1−O2	175.2(4)	C7−Pt1−O1	172.6(5)
C11−S1−C14	103.6(6)	O3−S1−O4	118.9(7)
Pt-PVS			
Pt1−N1	1.994(4)	Pt1−C7	1.987(5)
Pt1−O1	2.081(4)	Pt1−O2	2.001(4)
N1−Pt1−O2	176.04(16)	C7−Pt1−O1	172.83(19)
C11−S1−C14	103.4(3)		
Pt-PVB			
Pt1−N1	1.987(4)	Pt1−C7	1.998(5)
Pt1−O1	2.075(4)	Pt1−O2	2.009(4)
N1−Pt1−O2	176.74(16)	C7−Pt1−O1	171.89(18)
Pt-PVSi			
Pt1−N1	2.001(5)	Pt1−C7	1.981(6)
Pt1−O1	2.082(4)	Pt1−O2	1.985(4)
N1−Pt1−O2	175.0(2)	C7−Pt1−O1	174.2(2)
C26−Si1−C11	106.0(3)	C26−Si1−C14	110.7(3)
C11−Si1−C14	108.5(3)	C26−Si1−C20	107.8(3)
C11−Si1−C20	113.7(3)	C14−Si1−C20	110.0(3)
Pt-PVGe			
Pt1−N1	1.988(4)	Pt1−C7	1.983(5)
Pt1−O1	2.075(3)	Pt1−O2	1.994(3)
N1−Pt1−O2	175.47(15)	C7−Pt1−O1	173.47(18)
C26−Ge1−C11	105.7(2)	C26−Ge1−C14	109.9(2)
C11−Ge1−C14	109.1(2)	C26−Ge1−C20	107.9(2)
C11−Ge1−C20	113.7(2)	C14−Ge1−C20	110.5(2)

The stacking diagram in the crystal lattices of Pt-PVSO$_2$ and Pt-PVS are depicted in Figure 2 and Figure S1 (see Supporting Information). Obviously, the packing diagrams show a great difference between Pt-PVSO$_2$ and Pt-PVS. The Pt atoms in three adjacent molecules of complex Pt-PVSO$_2$ can form an isosceles triangle. The distance between the Pt1 atom and Pt2 atom is 8.5632(9) Å, quite close to the value of *a* of the Pt-PVSO$_2$ crystal cell, representing the base of the isosceles triangle. The location of the vertex Pt3 atom is as far as 6.2872(8) Å from Pt1 atom and Pt2 atom, suggesting the absence of intermolecular Pt···Pt interactions in complex Pt-PVSO$_2$. This can be ascribed to the pyridyl moiety in one Pt-PVSO$_2$ molecule that directly points to the central Pt atom of another adjacent complex molecule, resulting in a fold-line shape of two-dimensional (2D) packing diagram (Figure 2 and Supporting Information, Figure S1), which indicates no interplanar $\pi\cdots\pi$ interactions as well. However, in the crystal structure of Pt-PVS, the molecules adopt antiparallel two-molecule pair arrangement. In addition, the terminal phenyl rings in the two-molecule pair stay away from the each other, which would avoid steric hindrances. Thus, the interplanar $\pi\cdots\pi$ distances and Pt···Pt distances in the crystal structure of Pt-PVS are 3.3940(8) and 3.4756(3) Å, respectively, revealing the presence of intermolecular $\pi\cdots\pi$ and Pt···Pt interactions. Therefore, Pt-PVSO$_2$ crystallized in an orthorhombic space group, while Pt-PVS crystallized in a monoclinic space group.

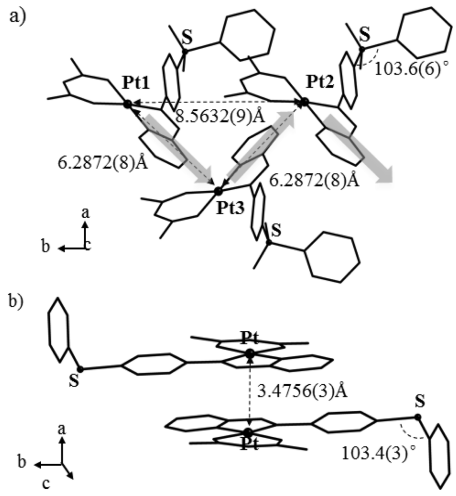

Figure 2. Crystal-packing diagram of (a) Pt-PVSO$_2$ and (b) Pt-PVS. (All hydrogen atoms are omitted for clarity.)

The crystal structure and the 2D stacking diagram in the crystal lattices of Pt-PVB are illustrated in Figure 3 and Supporting Information, Figure S2. The N1−Pt1−O2 and C7−Pt1−O1 angles are 176.74(16)° and 171.89(18)°, respectively, revealing a distorted square-planar geometry. The bond length of Pt1−O1 *trans* to vinyl carbon is much longer than that of Pt1−O2 *trans* to nitrogen atom (Pt1−O1 = 2.075(4) Å vs Pt1−O2 = 2.009(4) Å), and this difference is attributed to the stronger *trans* effect of vinyl carbon.

Although the Pt···Pt distance (3.6985(4) Å) in complex Pt-PVB stacked dimer is almost 1.0 Å shorter than that in similar B(Mes)$_2$-functionalized ppy-type platinum(II) complexes (where Mes = 2-morpholinoethanesulfonic acid),[37] the Pt···Pt interaction in the crystal of Pt-PVB is weaker compared with that in Pt-PVS (Pt···Pt distance ca. 3.4756(3) Å) due to the much stronger steric effect induced by the presence of the bulky B(Mes)$_2$ group. The interplanar $\pi\cdots\pi$ distance in the crystal structure of Pt-PVB is 3.5619(84) Å, which is shorter than the Pt···Pt distance. This can be ascribed to the slight deviation between the two platinum(II) centers.

The perspective views and crystal-packing diagrams of Pt-PVSi and Pt-PVGe (Figure 4 and Supporting Information, Figure S3) show that the crystal structures of these two complexes are almost identical. It can be expected that the bond length of C−Ge (ca. 1.95 Å) is longer than that of C−Si (ca. 1.87 Å) due to the larger radius of Ge atom compared with that of Si atom. All the C−Si−C and C−Ge−C angles are quite close to 109°28′, indicating that the four phenyl rings are located at the four vertexes of a slightly distorted tetrahedron. Consequently, the tetrahedral geometry induces a strong steric effect, resulting in the long Pt···Pt distances in the crystal structures of Pt-PVSi and Pt-PVGe (6.7669(5) Å and 6.7859(3) Å, respectively), indicating the negligible Pt···Pt interaction between each individual molecule (Supporting Information, Figure S3).

From all these results aforementioned, it is clear that not only the vinylpyridine-type platinum(II) complexes show different structural features from their ppy-type counterparts but also the main-group moieties can exert sound impact on the intermolecular interaction behaviors of the concerned complexes.

Electrochemical Properties. The electrochemical properties of these vinylpyridine-type platinum(II) complexes were investigated by cyclic voltammetry (CV) calibrated with ferrocene/ferrocenium (Fc/Fc$^+$) redox couple as an internal reference under nitrogen atmosphere. The results are presented

dx.doi.org/10.1021/ic502122t | *Inorg. Chem.* 2014, 53, 12986−13000

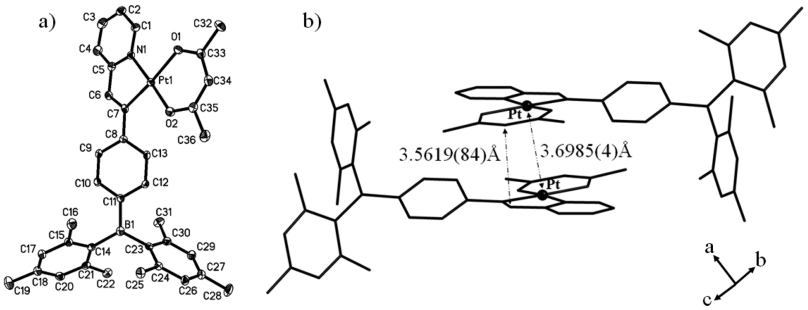

Figure 3. (a) Perspective views of Pt-PVB. Thermal ellipsoids are drawn at the 15% probability level. (b) Crystal-packing diagram of Pt-PVB. (All hydrogen atoms are omitted for clarity.)

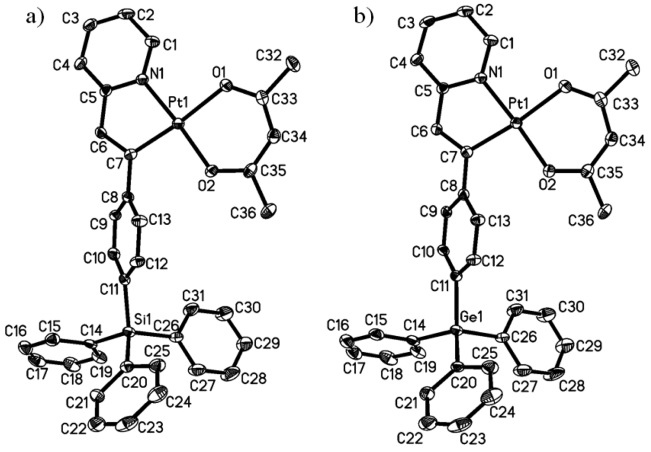

Figure 4. Perspective views of (a) Pt-PVSi and (b) Pt-PVGe. (All hydrogen atoms are omitted for clarity.) Thermal ellipsoids are drawn at the 15% probability level.

in Table 3. Different from the traditional ppy-type platinum(II) counterparts with typically one irreversible anodic peak

Table 3. Electrochemical Properties of the Platinum(II) Complexes[a]

	E_{pa} (V)	E_{pc} (V)	HOMO (eV)[b]	LUMO (eV)[c]
Pt-PVP	0.36, 0.48	−2.26	−5.16	−2.54
Pt-PVB	0.36, 0.52	−2.04, −2.24	−5.16	−2.76
Pt-PVSi	0.36, 0.48	−2.23	−5.16	−2.57
Pt-PVGe	0.36, 0.48	−2.25	−5.16	−2.55
Pt-PVN	0.30, 0.43	−2.30	−5.10	−2.50
Pt-PVPO	0.38, 0.50	−2.16, −2.23	−5.18	−2.64
Pt-PVO	0.37, 0.49	−2.26	−5.17	−2.54
Pt-PVS	0.35, 0.49	−2.29	−5.15	−2.54
Pt-PVSO$_2$	0.39, 0.51	−2.05, −2.21	−5.19	−2.75

[a]In acetonitrile solution using $[Bu_4N]BF_4$ as the supporting electrolyte, scan rate at 100 mV/s, vs. Fc/Fc^+ couple (ca. 4.8 eV vs vacuum). [b]HOMO levels are calculated according to the equation HOMO = −(4.8 + E_{pa}). [c]LUMO levels are obained according to the equation LUMO = −(4.8 + E_{pc}).

potential (ca. 0.5 V) ascribed to the oxidation of the Pt(II) centers,[25a,41] all the complexes show two irreversible oxidation processes (Supporting Information, Figure S4). Except in the case of Pt-PVN, the first anodic peak potential (E_{pa}) at ∼0.36 V should be assigned to the oxidation process associated with the electron-rich vinyl moieties in the complexes. The second E_{pa} at ∼0.5 V can be ascribed to the oxidation of the platinum(II) centers in these complexes.[25] For Pt-PVN, the first broad oxidation wave with E_{pa} at ca. 0.3 V might be assigned to the oxidation of both vinyl and triphenylamine groups, since our previous data about the ppy-type platinum(II) analogue is ca. 0.33 V for the oxidation of the triphenylamine moiety.[25] Obviously, bonding with electron-donating triphenylamine group will definitely make the vinyl moiety more easily oxidized. Apart from this, the Pt(II) center in Pt-PVN anchored with organic ligand showing strong electron-donating properties will be more inclined to be oxidized as well. So, Pt-PVN shows the lowest E_{pa} at ca. 0.30 and 0.43 V compared with the other complexes.

In the cathodic scan processes, all the complexes exhibit irreversible or quasi-reversible (ill-defined) reduction potential with the cathodic peak potential (E_{pc}) at ca. −2.25 V, which can be assigned to the reduction of the pyridyl moiety (Table 3).[18,25a] Attached to electron-donating groups, the pyridyl in Pt-PVN should be more reluctant to be reduced. So, Pt-PVN shows a more negative E_{pc} at ca. −2.30 V for the reduction of its pyridyl moiety in the ligand compared with other complexes (Table 3). Owing to its similar features to the triphenylamine unit, the SPh group also shows a more negative E_{pc} at ca. −2.29 V. For the complexes bearing electron-withdrawing groups, complexes Pt-PVB, Pt-PVPO, and Pt-PVSO$_2$ exhibit reduction waves at much less negative potential region with E_{pc} at ca. −2.04 V for Pt-PVB, ca. −2.16 V for Pt-PVPO, and ca. −2.05 V for Pt-PVSO$_2$. These reduction waves should be ascribed to the reducing of the electron-withdrawing groups B(Mes)$_2$, PO(Ph)$_2$, and SO$_2$Ph in the concerned complexes. Owing to the influence from these electron-withdrawing groups, the pyridyl rings in Pt-PVB, Pt-PVPO, and Pt-PVSO$_2$ are also easier to be reduced, indicated by the related reduction waves at less negative potential of ca. −2.24 V for Pt-PVB, ca. −2.23 V for Pt-PVPO, and ca. −2.21 V for Pt-PVSO$_2$, compared to that for the other complexes (Table 3).

Thermal and Photophysical Properties. The thermal properties data of these complexes investigated by thermogravimetric analysis (TGA) and differential scanning calorimetry (DSC) under nitrogen atmosphere are summarized in Table 4. The 5% weight-reduction temperatures of all these complexes range from 241 to 292 °C (Table 4), which is slightly lower than those of their ppy-type analogues.[18] The lower decomposing temperatures may result from the relatively weak Pt−C bonds indicated by the longer Pt−C bond lengths compared to those of their ppy-type analogues as aforementioned. The complexes bearing smaller main-group moieties, such as Pt-PVSO$_2$, Pt-PVS, and Pt-PVO, show slightly lower glass transition temperatures (T_g, ca. 125 °C) than the complexes with larger main-group moieties, such as Pt-PVSi and Pt-PVGe (ca. 150 °C) (Table 4). Although the T_g can be

dx.doi.org/10.1021/ic502122t | Inorg. Chem. 2014, 53, 12986−13000

Table 4. Photophysical and Thermal Properties for these Pt(II) Complexes

	absorption λ_{abs} (nm)[a]	emission λ_{em} (nm)[b] 298 K	emission λ_{em} (nm)[b] 77 K	Φ_p[c] (%)	k_r[d] (s^{-1})	k_{nr}[d] (s^{-1})	$\Delta T_{5\%}/T_g$[e] (°C)
Pt-PVP	258 (4.45), 306 (4.42), 376 (4.03), 410 (3.99), 431(3.42)	488 (10.4 ns), 629 (0.16 μs)	600 (0.88 μs), 650sh	1.3	1.5×10^4	1.1×10^6	241/135
Pt-PVB	278 (4.28), 336 (4.48), 418 (3.98), 444(2.97)	498 (14.1 ns), 667 (0.11 μs)	623 (0.65 μs), 682sh	1.2	1.8×10^4	1.5×10^6	275/141
Pt-PVSi	262 (4.30), 304 (4.24), 378 (3.76), 412 (3.80), 436(3.07)	486 (13.6 ns), 638 (0.25 μs)	604 (1.07 μs), 650sh	1.2	1.1×10^4	9.2×10^5	292/153
Pt-PVGe	258 (4.28), 304 (4.04), 378 (3.76), 412 (3.80), 435(3.10)	484 (2.4 ns), 634 (0.21 μs)	602 (0.95 μs), 650sh	1.3	1.3×10^4	1.0×10^6	290/150
Pt-PVN	256 (4.29), 304 (4.45), 364 (4.18), 432 (4.09)	516 (10.2 ns), 646 (0.37 μs)	620 (1.65 μs), 672sh	8.0	4.8×10^4	5.6×10^5	278/138
Pt-PVPO	264 (4.14), 306 (4.02), 382 (3.58), 410 (3.60), 435 (3.53)	472 (3.2 ns), 646 (0.14 μs)	620 (0.71 μs), 670sh	7.7	1.1×10^4	1.4×10^6	262/146
Pt-PVO	254 (4.45), 306 (4.42), 372 (3.93), 416 (3.95), 435 (3.88)	498 (5.1 ns), 632 (0.17 μs)	600 (1.06 μs), 652sh	1.8	1.7×10^4	9.2×10^5	272/123
Pt-PVS	256 (4.53), 316 (4.46), 376 (3.96), 414 (4.02), 437(3.33)	506 (2.5 ns), 640 (0.18 μs)	618 (1.11 μs), 674sh	1.7	1.5×10^4	8.8×10^5	275/125
Pt-$PVSO_2$	266 (4.31), 308 (4.17), 388 (3.61), 408 (3.77), 436 (3.69)	484 (1.6 ns), 654 (0.11 μs)	626 (0.47 μs), 686sh	0.5	1.1×10^4	2.1×10^6	262/128

[a]Measured in CH_2Cl_2 at room temperature; log ε values are shown in parentheses. [b]Measured in CH_2Cl_2 solutions at room temperature. The phosphorescence lifetime τ_p is shown in parentheses. [c]In degassed CH_2Cl_2 relative to *fac*-[Ir(ppy)$_3$] (Φ_p = 0.40). [d]k_r: radiative constant; k_{nr}: nonradiative constant. $k_r = \Phi_p/\tau_p$; $k_{nr} = (1 - \Phi_p)/\tau_p$. [e]$\Delta T_{5\%}$ is the 5% weight-reduction temperature and T_g is the glass transition temperature.

affected by the packing style of the concerned molecules in crystals, clearly the main-group moieties should represent the most easily movable parts in these complexes. From their pack mode in crystal (Supporting Information, Figures S1–S3), the crystal lattices have provided enough room for the movements of the main-group moieties. Hence, the glass transition processes associated with these platinum(II) complexes should be mainly up to the main-group moieties. As aformentioned, the complexes with larger main-group moieties show higher T_g, since higher temperatures are generally needed to cause movements of larger groups.

The absorption spectra of these complexes are depicted in Figure 5, while the pertinent photophysical data are summarized in Table 4. All of these complexes show two kinds of absorption bands in their UV–vis absorption spectra at 298 K (Figure 5). In general, the strong high-energy absorption bands (<ca. 360 nm) are assigned to the spin-allowed ligand-centered (LC) π–π^* transitions, which also can be proved by their large extinction coefficients (log ε > 4).[31] The much weaker, low-energy absorption bands are mainly centered after ca. 360 nm, which may be assigned to intraligand charge transfer (ILCT) and/or metal-to-ligand charge transfer (MLCT) transitions depending on the main-group substituents. Complex Pt-PVN, which contains a strong electron-donating NPh_2 group, shows a very strong low-energy absorption band with a peak at ~430 nm and extinction coefficient (ε) of ~1.24×10^4 dm^3 mol^{-1} cm^{-1}, which is assigned to the ILCT transition. It has been reported that a ruthenium(II) complex bearing a ligand containing electron-donating NPh_2 group and electron-accepting pyridyl moiety shows absorption band exceeding 350 nm due to the ILCT transition from NPh_2 group to pyridyl moiety.[42] In addition, as the theoretical calculation results suggested (vide infra), the Pt(II) center makes negligible contribution to the highest occupied molecular orbital (HOMO) of Pt-PVN, while the triphenylamine moiety makes the predominate contribution to the HOMO; thus, this low-energy absorption band should not result from the MLCT transitions but from the ILCT (triphenylamine moiety → pyridyl ring) transition. In complex Pt-PVS, the HOMO has significant electron density on the organic ligand (SPh group and vinyl moiety) as well as Pt(II) center; thus, the low-energy absorption band should be assigned to the mixing ILCT/MLCT (SPh and vinyl moiety/Pt(II) center → pyridyl ring) transitions. For complexes bearing weak electron-donating moieties, namely, Pt-PVP, Pt-PVO, Pt-PVSi, Pt-PVGe, and complexes bearing electron-withdrawing moieties, namely, Pt-PVPO and Pt-$PVSO_2$, their HOMOs are mainly distributed on the vinyl units and Pt(II) centers; therefore, the low-energy absorption bands should also be attributed to the mixing ILCT/MLCT (vinyl moieties/Pt(II) centers → pyridyl rings) transitions. Besides, the profiles of their low-energy absorption bands look like broad platforms, which also implies the mixture of ILCT/MLCT transitions. Although remarkable contributions from the vinyl unit and Pt(II) center to the HOMO of Pt-PVB are also revealed by the theoretical calculated results, the charge-transfer destination is no longer the pyridyl ring solely because the boron center is also capable of accepting the electron from the vinyl unit and Pt(II) center due to the strong electron-accepting character

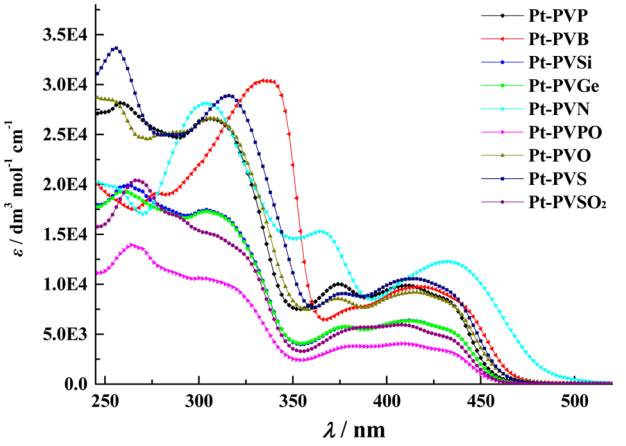

Figure 5. UV–vis absorption spectra of the platinum(II) complexes in CH_2Cl_2 solution recorded at 298 K.

dx.doi.org/10.1021/ic502122t | *Inorg. Chem.* 2014, 53, 12986–13000

induced by the vacant p_π orbital of B atom.[25,32] Therefore, the low-energy absorption band of Pt-PVB can be assigned to the mixing ILCT/MLCT (vinyl moiety/Pt(II) center → boron center) transition.

As depicted in Figure 6a, all of these complexes display two emission bands under UV irradiation at room temperature in

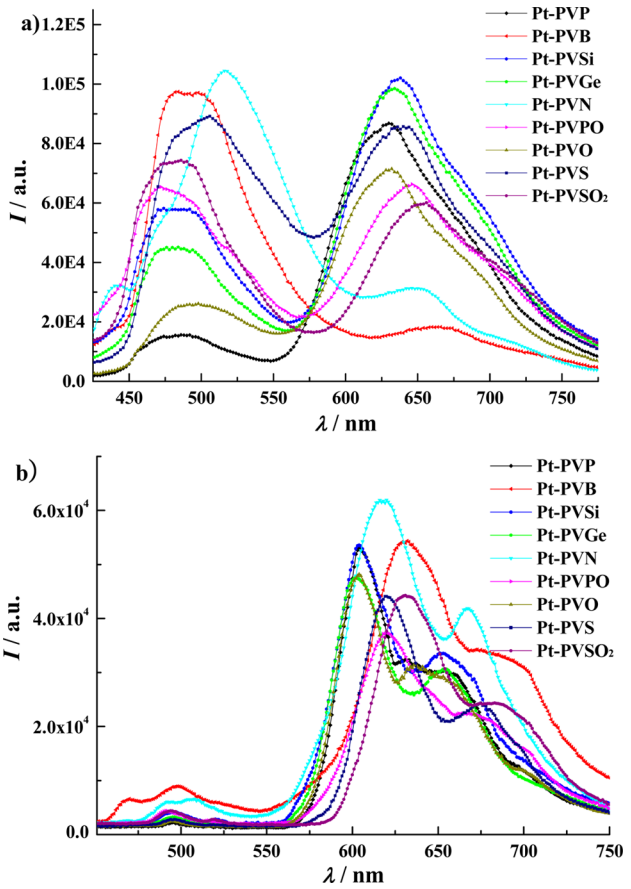

Figure 6. Photoluminescence (PL) spectra of the platinum(II) complexes in CH_2Cl_2 solution recorded at (a) 298 K and (b) 77 K.

CH_2Cl_2 solutions (Table 4). The high-energy emission band in the range from 472 to 516 nm can be safely assigned to the singlet-state emission due to the short lifetime (on the order of nanoseconds (<15 ns)) (Table 4). On the contrary, the emission band at much longer wavelength ranging from 629 to 667 nm can be attributed to the triplet-state emission due to the large Stokes shift (Figures 5 and 6), long lifetime (on the order of microseconds), and marked enhancement at 77 K (Figure 6b). Furthermore, the assignment of the emission bands is also supported by the fact that the intensities of these low-energy emissions are increased in the degassed solutions compared with that in aerated solutions, yet the intensities of the high-energy emission bands are almost identical in both degassed and aerated solutions (Supporting Information, Figure S5). Obviously, the phosphorescent emission was successfully induced by the spin−orbit coupling (SOC) effect due to the heavy atom effect associated with the Pt(II) center. Comparing the results in Figure 6, the phosphorescence spectra of the platinum(II) complexes show obvious rigidochromic effect: The phosphorescence bands are blue-shifted by 0.069−0.13 eV on going from 298 to 77 K. The rigidochromic shift associated with these complexes indicates charge-transfer features of the emissive triplet states involved in these complexes.[43a]

It is well-accepted that the photophysical properties of phosphorescent complexes show close relationship with excited states formed in the photoexcitation processes. From the time-dependent density functional theory (TD-DFT) calculation results (Table 5), it is clear that HOMO → LUMO (LUMO = lowest unoccupied molecular orbital) transitions of the platinum(II) complexes can represent the $S_0 \rightarrow S_1$ and/or $S_0 \rightarrow T_1$ transition processes due to the large coefficient over 0.5 in the configuration interaction (CI) of both S_1 and T_1 states as well as their large contributions to the transitions of $S_0 \rightarrow S_1$ and $S_0 \rightarrow T_1$ (Table 5), which generally indicate the emission behavior of molecules. Hence, we employ the molecular orbitals (MO) to explain the absorption and emission properties of the 2-vinylpyridine-type platinum(II) complexes. From the MO patterns obtained by theoretical computation (Figure 7), except for Pt-PVN, Pt-PVO, and Pt-PVS, the HOMOs of the complexes typically have major contributions from π orbitals of the vinyl moieties together with noticeable contributions from the d_π orbitals of metal centers, while the LUMOs are predominantly located on the π orbitals of the pyridine rings. So, the HOMO → LUMO transitions associated with the platinum(II) complexes show predominantly ligand-centered features (with intraligand charge-transfer (ILCT) characters) together with some MLCT characters. For Pt-PVN, Pt-PVO, and Pt-PVS, the HOMO → LUMO transitions exhibit almost totally the ligand-centered features with ILCT characters (Figure 7).[43b] As aforementioned, the HOMO → LUMO transition can represent the characters of both $S_0 \rightarrow S_1$ and $S_0 \rightarrow T_1$ transition processes. So, as indicated by their UV−vis absorption spectra, these complexes display two kinds of absorption bands, among which the strong absorption bands can be assigned to ligand-based $\pi-\pi^*$ transitions. From the HOMO patterns of the concerned complexes, the mixing of the d_π orbitals of metal centers and the π orbitals of the organic ligands can be clearly seen (Figure 7 and Table 5), indicating the SOC effect of the Pt(II) center in generating triplet states. So, the low-energy absorption features of the complexes except for Pt-PVN, Pt-PVO, and Pt-PVS should be induced mainly by the $^3\pi-\pi^*$ transitions with ILCT character mixed with some triplet MLCT (^{3}MLCT) features. For Pt-PVN, Pt-PVO, and Pt-PVS, their low-energy absorption features should predominantly come from the $^3\pi-\pi^*$ transitions with ILCT characters. Apart from the contributions from the $^3\pi-\pi^*$ transitions, the metal-perturbed $^1\pi-\pi^*$ transitions with ILCT feature can also contribute the weak absorption bands in the UV−vis absorption spectra of these complexes, since the metal perturbation can typically red-shift the $\pi-\pi^*$ transitions of the organic ligands in the platinum(II) complexes.[44a] The SOC effect induced by the heavy metal center is indicated by the similar oscillator strengths (less than a factor of 2 in their extinction coefficients) for the metal-perturbed $^1\pi-\pi^*$ and $^3\pi-\pi^*$ absorption bands (Table 4 and Figure 5).[43b]

Owing to the triplet states induced by the SOC effect, all these groups exhibit phosphorescence even at room temperature (Figure 6a). Bearing the organic ligands with longer conjugation compared with the ppy-type analogues, the HOMO → LUMO transitions involved in these complexes show mainly ligand-centered characters despite the contributions from the metal center (Figure 7). The MO patterns would clearly throw light on the weaker SOC effect induced by the Pt(II) center in these complexes compared with that

dx.doi.org/10.1021/ic502122t | Inorg. Chem. 2014, 53, 12986−13000

Table 5. DFT/TD-DFT Calculation Results for These Pt(II) Complexes

	contribution of metal d_π to HOMO[a]	contribution of metal d_π to LUMO[a]	the largest coefficient in the CI expansion of the T_1 state[b] (λ_{cal}/nm)	percentage contribution of H→L transition to the T_1 state[b]	the largest coefficient in the CI expansion of the S_1 state[b] (λ_{cal}/nm)	percentage contribution of H→L transition to the S_1 state[b]	the oscillator strength (f) of the $S_0 \rightarrow S_1$ transition
Pt-PVP	32.35%	10.08%	H→L: 0.665 57 (538.21 nm)	88.60%	H→L: 0.661 46 (401.86 nm)	87.50%	0.1010
Pt-PVB	32.07%	7.54%	H→L: 0.646 60 (554.34 nm)	83.62%	H→L: 0.656 38 (413.59 nm)	86.17%	0.2496
Pt-PVSi	31.66%	9.62%	H→L: 0.667 51 (543.92 nm)	89.11%	H→L: 0.661 20 (404.84 nm)	87.44%	0.1577
Pt-PVGe	31.55%	9.79%	H→L: 0.667 26 (542.98 nm)	89.05%	H→L: 0.662 00 (404.46 nm)	87.65%	0.1564
Pt-PVN	2.11%	9.50%	H→L: 0.541 30 (572.32 nm)	58.60%	H→L: 0.691 19 (450.88 nm)	95.55%	0.3702
Pt-PVPO	34.72%	9.51%	H→L: 0.663 23 (540.52 nm)	87.97%	H→L: 0.653 49 (402.55 nm)	85.41%	0.1406
Pt-PVO	20.05%	10.02%	H→L: 0.648 87 (545.67 nm)	84.21%	H→L: 0.662 37 (407.76 nm)	87.75%	0.1770
Pt-PVS	12.04%	9.55%	H→L: 0.525 00 (543.17 nm)	55.12%	H→L: 0.597 88 (405.68 nm)	71.49%	0.1771
Pt-$PVSO_2$	37.03%	9.07%	H→L: 0.655 76 (540.13 nm)	86.00%	H→L: 0.645 03 (401.89 nm)	83.21%	0.1400

[a]The data have obtained by exporting DFT results with the software AOMix. [b]H → L represents the HOMO to LUMO transition. CI stands for configuration interaction.

Figure 7. Plots of the HOMO (down) and LUMO (up) for each of these complexes. (All hydrogen atoms are omitted for clarity.)

involved in the traditional ppy-type analogues.[44b] Accordingly, besides the phosphorescence band at longer wavelength region, these complexes exhibit fluorescence band in their photoluminescence (PL) spectra due to the weaker SOC effect, which cannot convert all the singlet states into triplet ones (Figure 6a). So, there are two emission bands appearing in the PL spectra of the platinum(II) complexes (Figure 6a). Their fluorescence bands show very similar line shape and energy level to those of the corresponding organic ligands (Supporting Information, Figure S6). Hence, the high-energy emissions should come from the metal-perturbed $^1\pi-\pi^*$ states of the organic ligand with ILCT characters, which is supported by the MO patterns of these complexes as well (Figure 7). The excitation spectra for the fluorescence band of these platinum(II) complexes were obtained as well (Supporting Information, Figure S7). However, the preferred excitation wavelength for the fluorescence band locates at ca. 430 nm, exhibiting obvious red-shift effect compared with the absorption maximum of the corresponding organic ligands (Supporting Information, Figure S8). This can be ascribed to the fact that the metal perturbation in these complexes shifted the $^1\pi-\pi^*$ transition of the organic ligand with ILCT characters to the longer wavelength region, which has been frequently observed in the platinum(II) complexes.[44a] As indicated by the HOMO → LUMO transitions (Figure 7), the phosphorescence band should show predominantly ligand-centered $^3\pi-\pi^*$ features with ILCT characters for Pt-PVN, Pt-PVO, and Pt-PVS and $^3\pi-\pi^*$ mixed with some ^{3}MLCT character for the remaining complexes. Hence, the PL spectra of these complexes exhibit obvious vibrational features at 77 K (Figure 6b).

Compared with the corresponding ppy-type counterparts, these 2-vinylpyridine-type ligands possess longer conjugation, which will induce $^1\pi-\pi^*$ states in a lower energy level and thus low-energy $^3\pi-\pi^*$ states.[44c] Therefore, these platinum(II)

dx.doi.org/10.1021/ic502122t | Inorg. Chem. 2014, 53, 12986−13000

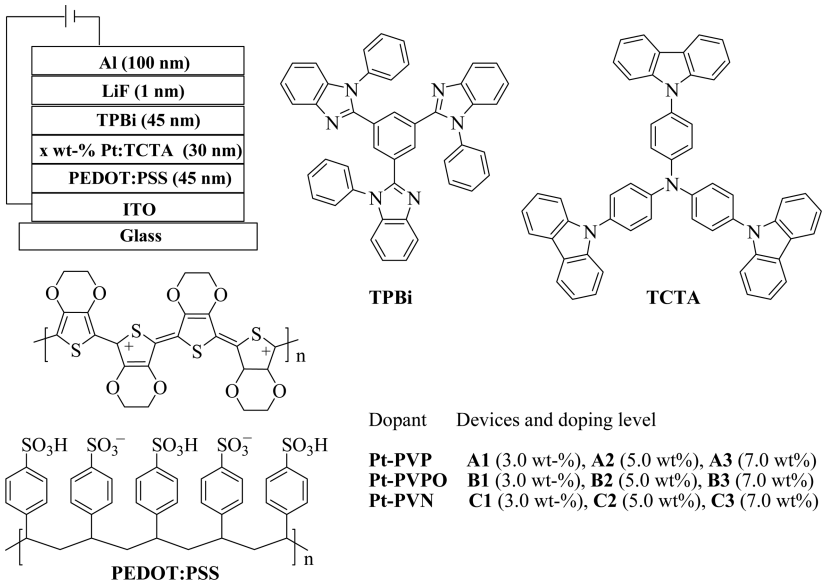

Figure 8. Configuration of the electrophosphorescent OLEDs and the chemical structures of the key chemicals involved.

complexes emit phosphorescence with much longer wavelength (>629 nm) (Figure 6a) compared with their ppy-type counterparts in the literature.[25] Taking Pt-PVP as the reference complex with the triplet emission peak at 629 nm (298 K), Pt-PVSi and Pt-PVGe, with main-group $SiPh_3$ and $GePh_3$ showing obviously neither electron-donating nor electron-withdrawing character, exhibit slightly red-shifted emissions (ca. 638 and 634 nm, respectively), revealing the trivial effects of substituent on photophysical properties due to the feeble electron-donating abilities of the sp^3-hybridized Si and Ge atoms. Bearing main-group moieties with electron-donating features, Pt-PVN (λ_{em} = ca. 646 nm), Pt-PVS (λ_{em} = ca. 640 nm), and Pt-PVO (λ_{em} = ca. 632 nm) all show bathochromic emission with respect to that of the reference complex Pt-PVP (λ_{em} = ca. 629 nm). Pt-PVN contains the organic ligand anchored with NPh_2 group showing strong electron-donating character indicated by its substantial contribution to the HOMO of Pt-PVN. Hence, the electron-donating NPh_2 group will both lift the HOMO level to generate narrower bandgap of Pt-PVN and facilitate the excitation process to form excited states in a lower energy level, which induces bathochromic effect in both the absorption (Figure 5) and emission bands (Figure 6 and Table 4) of Pt-PVN with respect to that of Pt-PVP. Similarly, the bathochromic effect in the emission of Pt-PVS can be ascribed to both the more polarizable and electron-donating character of the S atom, leading to an enhanced conjugative effect and a higher HOMO level to facilitate the formation of excited states in lower energy level as well. Despite O and S being in the same group, Pt-PVO shows slightly longer emission wavelength (ca. 632 nm) than the reference complex Pt-PVP (ca. 629 nm) and shorter emission wavelength compared with Pt-PVS (ca. 640 nm), because of the inherently weak π-donating ability of O atom as indicated by its much lower contribution to the HOMO of Pt-PVO (ca. 1.3%) than that of S atom to the HOMO of Pt-PVS (ca. 4.3%).

According to their HOMO patterns (Figure 7), it is reasonable that bathochromic effect will be generally induced through introducing the electron-donating group to vinyl moiety in the organic ligands.[45] However, with the electron-withdrawing organoboryl group attached to the vinyl moiety, Pt-PVB exhibits obviously red-shifted emission maxima at ca. 667 nm compared with the reference complex Pt-PVP (ca. 629 nm) and even Pt-PVN (ca. 646 nm) with strong electron-donating group. The HOMO pattern of Pt-PVB is similar to that of Pt-PVP (Figure 7). Hence, the explanation of the bathochromic effect in the emission maxima of Pt-PVB cannot be found from its HOMO character. However, the TD-DFT calculation indicated that the HOMO → LUMO transition can represent the emissive T_1 character (i.e., ligand-centered $^3\pi-\pi^*$) of Pt-PVB as aforementioned. So, the answer to this question might only lie in the LUMO of Pt-PVB, which shows noticeable difference from that of Pt-PVP (Figure 7). The p_π orbital of the B atom makes a noticeable contribution to the LUMO of Pt-PVB (ca. 16.6%), indicating that significant electron density would be transferred to the $B(Mes)_2$ moiety from the chelated vinyl group together with subordinate contribution from iridium(III) center in the charge transfer (CT) process of Pt-PVB. In contrast, the CT processes in other complexes are oriented toward the pyridyl moiety (Figure 7). Owing to the strong π-accepting character of the "empty" p_π orbital, the $B(Mes)_2$ moiety will tend to lower the LUMO level of Pt-PVB as confirmed by CV data (Table 3) and hence facilitate the HOMO → LUMO transition, which will stabilize the triplet states strongly, in agreement with the more red-shifted weak absorption band reflecting the formation of triplet state (Figure 5 and Table 4). As a result, the low-energy ligand-centered triplet state of Pt-PVB leads to a longer emission wavelength at ca. 667 nm. Different from the $B(Mes)_2$ moiety showing strong π-accepting character, the SO_2Ph and $POPh_2$ complexes exhibit inductively electron-withdrawing property, which cannot render them as ideal destinations for electrons in the CT processes in Pt-PVSO$_2$ and Pt-PVPO, as indicated by the negligible contribution to the LUMOs of Pt-PVSO$_2$ and Pt-PVPO from SO_2Ph and $POPh_2$, respectively. However, the strong electron-withdrawing character of the polar O═S═O and P═O units will help in lowering the LUMO levels of Pt-PVSO$_2$ and Pt-PVPO, yet the ability of SO_2Ph and $POPh_2$ in lowering the LUMO levels is weaker than that of the $B(Mes)_2$ moiety, which has been confirmed by the CV measurement (Table 3). The low LUMO levels of Pt-PVSO$_2$ and Pt-PVPO

dx.doi.org/10.1021/ic502122t | Inorg. Chem. 2014, 53, 12986−13000

will also make the HOMO → LUMO transition easier to form ligand-centered $^3\pi-\pi^*$ states in a lower energy level. Accordingly, Pt-PVSO$_2$ and Pt-PVPO show longer emission wavelengths (ca. 654 and 646 nm, respectively) than the reference complex Pt-PVP (ca. 629 nm), but shorter emission wavelengths with respect to Pt-PVB (ca. 667 nm).

These vinylpyridine-type platinum(II) complexes show mediocre PL Φ values in CH_2Cl_2 at room temperature (Table 4). The values of the radiative constant (k_r) and nonradiative constant (k_{nr}) for all these complexes are also listed in Table 4 to characterize the emission properties. The value of k_{nr} for these complexes is almost 2 orders of magnitude larger than that of k_r, indicating the presence of more efficient nonradiative decay pathways. In the conventional ppy-type Pt(II) complexes, the central Pt(II) ion is directly coordinated to the carbon atom on the phenyl ring linked to pyridyl unit, which will prevent the phenyl ring from rotating and lock the phenyl ring to keep a coplanar conformation with the pyridyl ring, thereby enhancing the molecular rigidity. Generally, increasing molecular rigidity can benefit the radiative decay pathways.[2] However, as the X-ray crystal structure revealed, the central Pt(II) ion in the vinylpyridine-type complex is coordinated to the vinyl carbon atom, leaving the freedom of the phenyl ring and main-group units to rotate along the single C−C bond linked to the vinyl moiety, which may increase the chances for the nonradiative decay and decrease the PL quantum yields. Besides their smaller radiative decay constant, the ligand-centered phosphorescent character might be another reason for the low Φ_P of these complexes.[46]

Tuning of Electrophosphorescent Behavior by Main-Group Moieties. Owing to the fact that these kinds of Pt(II) complexes have not been applied to phosphorescent OLEDs (PHOLEDs), their electrophosphorescent properties were characterized in this section to show the influence of main-group moieties with different electronic characters on their electrophosphorescent behavior. Among all these complexes, the parent complex Pt-PVP, Pt-PVPO with electron-withdrawing group, and Pt-PVN with electron-donating moiety were selected to evaluate their EL potentials, since the three complexes could represent the electronic features of all the complexes. The OLEDs were constructed with cheap solution process, adopting the simple configuration of ITO/PEDOT:PSS (45 nm)/*x* wt % Pt:TCTA (30 nm)/TPBi (45 nm)/LiF:Al (1:100 nm) (Figure 8). The thin PEDOT:PSS layer serves the purpose of hole injection. The host material for the phosphorescent dopant is 4,4′,4″-tri(*N*-carbazolyl)-triphenylamine (TCTA). For its excellent electron transporting (ET) ability and low HOMO level of ca. 6.3 eV, 1,3,5-tris(*N*-phenylbenzimidazol-2-yl)benzene (TPBi) can fulfill the function of both an electron transporting layer (ETL) and a hole blocking layer (HBL), whereas LiF serves as the electron injection layer (EIL). With the aim of optimizing the EL performances, OLEDs with different doping levels were fabricated as well (Figure 8).

At proper driving voltage, all the devices emit intense red phosphorescence (Figure 9 and Supporting Information, Figure S9). For the device A2, the EL maximum locates at ca. 628 nm, while those for device B2 and C2 are 644 and 648 nm, respectively. Besides the EL band at deep red region, there are high-energy EL peaks at ca. 516 nm for the devices using Pt-PVN as emitter (Figure 9 and Supporting Information, Figure S9). The high-energy EL might come from the $^1\pi-\pi^*$ state of the ligand due to the much weaker SOC effect in Pt-PVN.

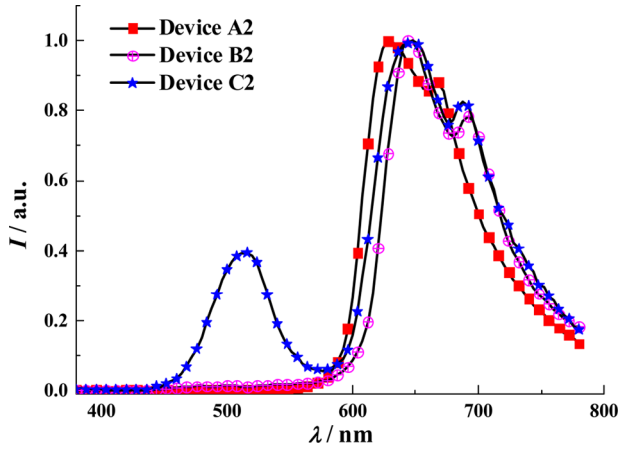

Figure 9. EL spectra for the optimized electrophosphorescent OLEDs at ∼10 V.

The related EL results for the devices A2, B2, and C2 are summarized in Table 6, and performances for all the devices are shown in Supporting Information, Table S1. The representative current density−voltage−luminance (*J*−*V*−*L*) characteristics for the optimized devices A2, B2, and C2 are shown in Figure 10 (also see Supporting Information, Figure S10 for other devices). The red-emitting device A2 doped with Pt-PVP shows a turn-on voltage of 4.8 V, a maximum brightness (L_{max}) of 6084 cd m^{-2} at 16.6 V, peak external quantum efficiency (η_{ext}) of 0.88%, luminance efficiency (η_L) of 5.79 cd A^{-1}, and power efficiency (η_p) of 2.42 lm W^{-1} (Table 6 and Supporting Information, Figure S11). Encouragingly, the deep red-emitting device B2 with Pt-PVPO can exhibit even better EL performances with L_{max} of 2955 cd m^{-2} at 12.6 V and EL efficiencies of 1.61%, 6.92 cd A^{-1}, and 2.21 lm W^{-1}, respectively (Table 6 and Figure 11). However, the device C2 shows inferior EL ability (η_{ext} of 0.29%, η_L of 2.48 cd A^{-1}, and η_P of 1.10 lm W^{-1}) compared with devices A2 and B2 (Table 6 and Supporting Information, Figure S11). From the EL results for devices A2, B2, and C2, it might be concluded that the phosphorescent emitter with electron-withdrawing group (Pt-PVPO) can show better EL performances, while the one with electron-donating moiety (Pt-PVN) exhibits inferior potential. This result can be explained as follows: from the CV results aforementioned (Table 3), these complexes can show good hole injection features due to their high-lying HOMO levels. It can be expected that Pt-PVPO will exhibit good electron injection/transporting behavior because of its low-lying LUMO level, which will lead to balanced injection/transporting ability for both kinds of charge carriers in the device. On the contrary, considering the good hole injection/transporting ability of Pt-PVN induced by the NPh_2 group, the severe unbalanced charge carrier injection/transporting can be expected in the device based on Pt-PVN. Hence, Pt-PVPO with balanced charge carrier injection/transporting features can outperform Pt-PVN and Pt-PVP in EL characterization. The more unbalanced charge carrier injection/transporting properties of the device based on Pt-PVN makes it even show inferior EL performances compared with devices based on Pt-PVP and Pt-PVPO. Although devices based on these three complexes show relatively low η_{ext} due to their low Φ_P, their deep-red EL can show CIE coordinates (Table 6 and Supporting Information, Table S1) very close to the NTSC-recommended standard red CIE coordinates of (0.67, 0.33).[47] The documented deep-red

dx.doi.org/10.1021/ic502122t | Inorg. Chem. 2014, 53, 12986−13000

Table 6. EL Performance of the Solution-Processed Devices A2, B2, and C2

device	dopant	$V_{turn\text{-}on}$ (V)	luminance L_{max} (cd m^{-2})[a]	η_{ext} (%)	η_L (cd A^{-1})	η_p (lm W^{-1})	λ_{max} (nm)[d]
A2	Pt-PVP (5.0 wt %)	4.8	6084 (16.6)	0.88 (8.2)[a]	5.79 (8.2)	2.42 (6.8)	628
				0.87[b]	5.69	2.29	(0.68, 0.32)
				0.86[c]	5.63	1.70	
B2	Pt-PVPO (5.0 wt %)	4.8	2955 (12.6)	1.61 (10.2)	6.92 (10.2)	2.21 (9.5)	644
				0.90	4.25	1.75	(0.67, 0.32)
				1.54	6.70	2.19	
C2	Pt-PVN (5.0 wt %)	4.2	750 (12.6)	0.29 (7.8)	2.48 (7.8)	1.10 (6.5)	516, 648
				0.27	2.35	1.08	(0.49, 0.41)
				0.26	2.20	0.75	

[a]Maximum values of the devices. Values in parentheses are the voltages at which they were obtained. [b]Values were collected at 20 mA cm^{-2}. [c]Values collected at 100 cd m^{-2}. [d]Values were collected at 12 V and CIE coordinates (x, y) are shown in parentheses.

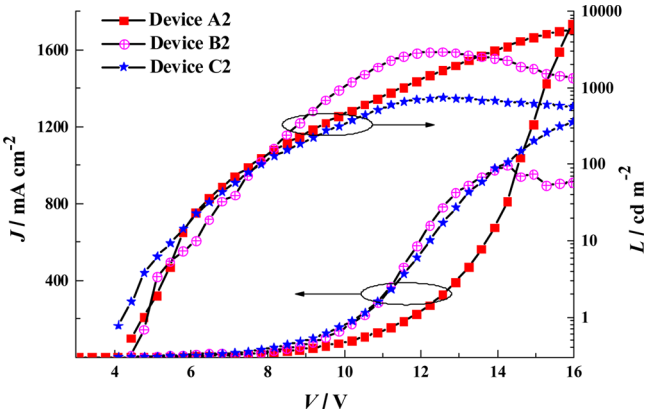

Figure 10. J–V–L curves for the optimized devices A2, B2, and C2.

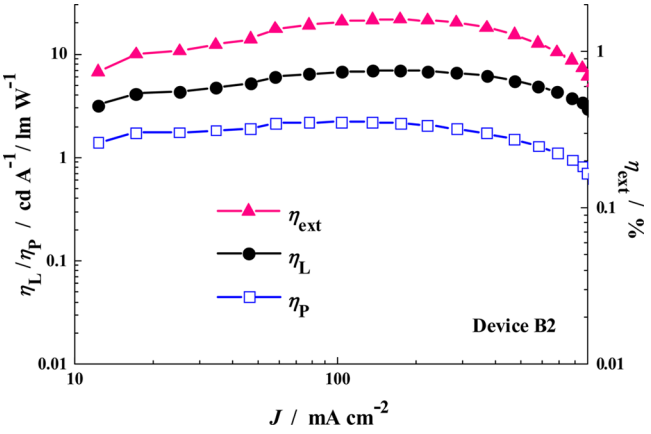

Figure 11. Relationship between EL efficiencies and current density for device B2.

EL devices based on Pt(II) complexes with the x-component of CIE equal to and/or exceeding 0.67 are relatively rare.[48] Besides, the device based on Pt-PVPO gives a high η_L value of 6.92 cd A^{-1} and η_P value of 2.21 lm W^{-1}, which are even higher or comparable to those of devices based on iridium(III) complexes[49] and ruthenium(II) complexes[50] displaying similar CIE coordinates, rendering the device based on Pt-PVPO among the best deep-red emission PHOLEDs in terms of the luminance efficiency and power efficiency. For example, a deep red-emitting device based on bis(8-hydroxyquinolato)platinum-(II) complex can give η_{ext} of 1.7% and η_L of 0.32 cd A^{-1}.[48a] With the CIE of (0.678, 0.317), the device based on an Ir(III) complex shows η_P of 0.32 lm W^{-1} and η_L of 1.25 cd A^{-1},[49e] and another solution-processed red-emitting Ir(III) dendrimer-based device achieves η_P of 1.3 lm W^{-1} and η_L of 3.3 cd A^{-1} with the CIE of (0.67, 0.33).[49f] Deep-red EL devices using neutral Ru(II) emitters can realize high η_P of 2.36 lm W^{-1} with η_L of 5.08 cd A^{-1} and η_P of 2.74 lm W^{-1} with η_L of 8.02 cd A^{-1}, respectively.[50] Therefore, these vinylpyridine-type Pt(II) complexes are promising for fabricating solution-processed deep red-emitting PHOLEDs with CIE coordinates close to the standard red point as well as attractive luminance efficiency and power efficiency.

CONCLUSIONS

A prominent class of phosphorescent 2-vinylpyridine-type platinum(II) complexes bearing various main-group moieties was designed and synthesized for the first time. Their structural, thermal, photophysical, electrochemical, and electroluminescent properties were also presented. The main-group moieties can exert sound impact on both the molecular packing mode of these complexes in solid state and the emission maxima. Because of the electronic characters of the corresponding 2-vinylpyridine-type ligands, these complexes exhibit their unique photophysical, electrochemical, and electroluminescent characters with respect to their ppy-type analogues. Furthermore, the combined electronic features from both the organic ligands and main-group moieties can furnish the concerned complexes with balanced charge carrier injection/transporting behaviors to benefit the EL efficiencies of the complexes. Deep red electroluminescent devices based on the 2-vinylpyridine-type Pt(II) complexes can give CIE coordinates very close to the NTSC recommended standard red CIE coordinates of (0.67, 0.33). Furthermore, the device also achieves high η_L of 6.92 cd A^{-1} and η_P of 2.21 lm W^{-1}, which are among the highest efficiencies obtained by PHOLEDs with CIE$_x$ $\geq$ 0.67. These results will not only give deep insight into the optoelectronic features of these new complexes but also provide the structure–property relationship information, which will definitely benefit the development of new platinum(II) phosphorescent complexes with great potential for important applications.

EXPERIMENTAL SECTION

General Information. All commercially available starting materials were used directly with no further purification. The solvents were carefully dried prior to use. All reactions were monitored using thin-layer chromatography (TLC) purchased from Merck & Co., Inc. Flash column chromatography and preparative TLC were made from silica gel bought from Shenghai Qingdao (200–300 mesh). ^{1}H, ^{13}C, and ^{31}P NMR spectra were recorded in $CDCl_3$ on a Bruker Avance 400 MHz spectrometer, and chemical shifts were referenced to the solvent residual peak at δ 7.26 for ^{1}H and 77.0 for ^{13}C, respectively. H_3PO_4

dx.doi.org/10.1021/ic502122t | Inorg. Chem. 2014, 53, 12986–13000

was used in the ^{31}P NMR study as external reference. Elemental analyses were preformed on a Flash EA 1112 elemental analyzer. The thermal gravimetric analysis (TGA) and differential scanning calorimetry (DSC) data were collected on a NETZSCH STA 409C instrument and a NETZSCH DSC 200 PC unit, respectively. UV−vis absorption spectra were measured at room temperature on a Shimadzu UV-2250 spectrophotometer. Emission spectra and lifetimes of these complexes were recorded on an Edinburgh Instruments Ltd. (FLSP920) fluorescence spectrophotometer using the software package provided by Edinburgh Instruments. The Φ_P values were determined in CH_2Cl_2 solutions at 298 K against *fac*-[Ir(ppy)$_3$] standard (Φ_P = 0.40).[51] Emission spectra of these complexes at 77 K were tested in CH_2Cl_2 matrix frozen by liquid nitrogen. Cyclic voltammetry was performed using a Princeton Applied Research model 273A potentiostat at a scan rate of 100 mV s^{-1}. All experiments were carried out in a three-electrode compartment cell with a Pt-sheet counter electrode, a glassy carbon working electrode, and a Pt-wire reference electrode. The supporting electrolyte used was 0.1 M [nBu$_4$N]BF$_4$ solution in acetonitrile. Fast atom bombardment (FAB) mass spectra were recorded on a Finnigan MAT SSQ710 system.

X-ray Crystallography. Single crystals of Pt-PVSO$_2$, Pt-PVS, Pt-PVB, Pt-PVSi, and Pt-PVGe of suitable dimensions were mounted in thin glass fibers for collecting the intensity data on a Bruker SMART CCD diffractometer (Mo Kα radiation and λ = 0.710 73 Å) in Φ and ω scan modes at 292 K. Their structures were solved by direct methods followed by difference Fourier syntheses and then refined by full-matrix least-squares techniques against F^2 using SHELXL-97[52] program on a personal computer. The positions of hydrogen atoms were calculated and refined isotropically using a riding model. All other non-hydrogen atoms were refined isotropically. Absorption corrections were applied using SADABS.[53]

Computational Details. Geometrical optimizations were conducted using the popular B3LYP functional theory. The basis set used for C, H, N, O, B, S, P, Ge, and Si atoms was 6-311G(d, p), while effective core potentials with a LanL2DZ basis set were employed for Pt atoms.[54,55] The energies of the excited states of the complexes were computed by TD-DFT based on all the ground-state geometries. All calculations were carried out by using the Gaussian 09 program.[56]

General Procedure for Synthesis of These Vinylpyridine-type Ligands. Under a nitrogen atmosphere, 2-vinylpyridine (1.1 mmol), the respective main-group element-substituted aryl halides (1.0 mmol), and the catalyst Pd(PPh$_3$)$_2$Cl$_2$ (0.1 mmol) were added in triethylamine (20 mL). The mixture was heated to 100 °C and stirred for 16−19 h. After the mixture cooled to room temperature, the solvent was removed, and the residual was purified on a silica column with a mixture of solvents of petroleum ether (bp 60−90 °C)/dichloromethane/diethyl ether (PE/DCM/DE) to give the title ligands.

L-PVP (solvent volume ratio V_{PE}/V_{DCM} = 1:4, Yield 64.8%) The spectral data were in accordance with those reported in the literature.[57]

L-PVB (V_{PE}/V_{DCM} = 1:2, Yield 69.2%) ^1H NMR (400 MHz, $CDCl_3$): δ (ppm) 8.61 (d, J = 4.4 Hz, 1H), 7.68−7.63 (m, 2H), 7.56−7.51 (m, 4H), 7.41 (d, J = 8.0 Hz, 1H), 7.26 (d, J = 16.0 Hz, 1H), 7.15 (t, J = 6.0 Hz, 1H), 6.83 (s, 4H), 2.31 (s, 6H), 2.02 (s, 12H); ^{13}C NMR (100 MHz, $CDCl_3$): δ (ppm) 155.36, 149.71, 145.90, 141.65, 140.77, 139.88, 138.60, 136.90, 136.55, 132.49, 129.41, 128.13, 126.61, 122.26, 122.24, 23.44, 21.21; FAB-MS (m/z): 429 $[M]^+$; Anal. Calcd for $C_{31}H_{32}BN$: C, 86.71; H, 7.51; N, 3.26; found: C, 86.60; H, 7.73; N, 3.32%.

L-PVSi (V_{PE}/V_{DCM} = 1:3, Yield 48.6%) ^1H NMR (400 MHz, $CDCl_3$): δ (ppm) 8.61 (dd, J = 0.8 Hz, 4.8 Hz, 1H), 7.68−7.62 (m, 2H), 7.59−7.57 (m, 10H), 7.46−7.36 (m, 10H), 7.31 (d, J = 16.4 Hz, 1H), 7.17−7.13 (m, 1H); ^{13}C NMR (100 MHz, $CDCl_3$): δ (ppm) 155.46, 149.69, 137.70, 136.77, 136.56, 136.36, 134.59, 134.03, 132.51, 129.63, 128.64, 127.89, 126.45, 122.23, 122.18; FAB-MS (m/z): 439 $[M]^+$; Anal. Calcd for $C_{31}H_{25}NSi$: C, 84.69; H, 5.73; N, 3.19; found: C, 84.55; H, 5.91; N, 3.03%.

L-PVGe (V_{PE}/V_{DCM} = 1:6, Yield 63.2%) ^1H NMR (400 MHz, $CDCl_3$): δ (ppm) 8.61 (d, J = 4.8 Hz, 1H), 7.68−7.60 (m, 2H), 7.58−7.54 (m, 10H), 7.44−7.34 (m, 10H), 7.20 (d, J = 16.0 Hz, 1H), 7.19−7.14 (m, 1H); ^{13}C NMR (100 MHz, $CDCl_3$): δ (ppm) 155.50, 149.68, 137.31, 136.63, 136.55, 135.93, 135.75, 135.36, 132.55, 129.15, 128.43, 128.29, 126.81, 122.19, 122.14; FAB-MS (m/z): 485 $[M]^+$; Anal. Calcd for $C_{31}H_{25}NGe$: C, 76.90; H, 5.20; N, 2.89; found: C, 76.77; H, 5.31; N, 2.75%.

L-PVN (V_{PE}/V_{DCM} = 1:3, Yield 43.7%) ^1H NMR (400 MHz, $CDCl_3$): δ (ppm) 8.57 (d, J = 4.0 Hz, 1H), 7.63 (t, J = 8.0 Hz, 1H), 7.57 (d, J = 16.0 Hz, 1H), 7.44 (d, J = 8.4 Hz, 2H), 7.35 (d, J = 8.0 Hz, 1H), 7.29−7.25 (m, 4H), 7.13−7.09 (m, 5H), 7.07−7.03 (m, 5H); ^{13}C NMR (100 MHz, $CDCl_3$): δ (ppm) 155.98, 149.61, 148.03, 147.40, 136.44, 132.22, 130.50, 129.31, 128.00, 126.07, 124.76, 123.26, 123.01, 121.77, 121.64; FAB-MS (m/z): 348 $[M]^+$; Anal. Calcd for $C_{25}H_{20}N_2$: C, 86.17; H, 5.79; N, 8.04; found: C, 85.98; H, 5.72; N, 7.96%.

L-PVPO ($V_{PE}/V_{DCM}/V_{DE}$ = 1:1:1, Yield 64.2%) ^1H NMR (400 MHz, $CDCl_3$): δ (ppm) 8.61 (d, J = 4.4 Hz, 1H), 7.72−7.64 (m, 10H), 7.55 (t, J = 7.2 Hz, 2H), 7.50−7.46 (m, 4H),7.39 (d, J = 8.0 Hz, 1H), 7.25 (d, J = 16.4 Hz, 1H), 7.18 (t, J = 6.0 Hz, 1H); ^{13}C NMR (100 MHz, $CDCl_3$): δ (ppm) 154.82, 149.74, 140.13, 136.66, 132.88, 132.52, 132.42, 132.07, 131.97, 131.93, 131.85, 131.32, 130.07, 128.55, 128.43, 127.00, 126.87, 122.61, 122.57; ^{31}P NMR (161.9 MHz, $CDCl_3$): δ (ppm) 28.99; FAB-MS (m/z): 381 $[M]^+$; Anal. Calcd for $C_{25}H_{20}NOP$: C, 78.73; H, 5.29; N, 3.67; found: C, 78.69; H, 5.31; N, 3.45%.

L-PVO (V_{PE}/V_{DCM} = 0:1, Yield 64.9%) ^1H NMR (400 MHz, $CDCl_3$): δ (ppm) 8.60 (d, J = 4.8 Hz, 1H), 7.64 (t, J = 6.0 Hz, 1H), 7.61 (d, J = 15.6 Hz, 1H), 7.54 (d, J = 8.0 Hz, 1H), 7.39−7.34 (m, 4H), 7.15 7.10 (m, 3H), 7.06−6.99 (m, 4H); ^{13}C NMR (100 MHz, $CDCl_3$): δ (ppm) 155.62, 149.61, 136.51, 131.86, 131.65, 129.78, 128.69, 128.49, 127.06, 126.86, 123.56, 121.96, 121.89, 119.20, 118.72; FAB-MS (m/z): 273 $[M]^+$; Anal. Calcd for $C_{19}H_{15}NO$: C, 83.49; H, 5.53; N, 5.12; found: C, 83.35; H, 5.56; N, 4.99%.

L-PVS (V_{PE}/V_{DCM} = 1:1,Yield 75.1%) ^1H NMR (400 MHz, $CDCl_3$): δ (ppm) 8.60 (d, J = 4.4 Hz, 1H), 7.66 (t, J = 8.0 Hz, 1H), 7.59 (d, J = 16.0 Hz, 1H), 7.50 (d, J = 7.6 Hz, 2H), 7.41−7.28 (m, 8H), 7.16−7.13 (m, 2H); ^{13}C NMR (100 MHz, $CDCl_3$): δ (ppm) 155.37, 149.67, 136.56, 136.40, 135.21, 131.78, 131.60, 130.53, 129.28, 128.70, 127.72, 127.39, 122.20, 122.12; FAB-MS (m/z): 289 $[M]^+$; Anal. Calcd for $C_{19}H_{15}NS$: C, 78.86; H, 5.22; N, 4.84; found: C, 78.59; H, 5.41; N, 4.85%.

L-PVSO$_2$ (V_{PE}/V_{DE} = 1:1, Yield 66.8%) ^1H NMR (400 MHz, $CDCl_3$): δ (ppm) 8.62 (d, J = 4.4 Hz, 1H), 7.96 (d, J = 8.0 Hz, 2H), 7.93 (d, J = 8.4 Hz, 2H), 7.81 (d, J = 8.0 Hz, 1H), 7.71−7.64 (m, 4H), 7.52 (d, J = 7.2 Hz, 2H), 7.38 (d, J = 7.6 Hz, 1H), 7.23−7.18 (m, 2H); ^{13}C NMR (100 MHz, $CDCl_3$): δ (ppm) 154.49, 149.85, 141.57, 136.74, 133.19, 131.35, 130.52, 129.30, 129.10, 128.83, 128.15, 127.61, 127.36, 127.30, 122.87; FAB-MS (m/z): 321 $[M]^+$; Anal. Calcd for $C_{19}H_{15}NO_2S$: C, 71.00; H, 4.70; N, 4.36; found: C, 69.79; H, 4.81; N, 4.28%.

General Procedure for Synthesis of These Vinylpyridine-type Platinum(II) Complexes. Under a nitrogen atmosphere, ligands (1.1 mmol) and K_2PtCl_4 (1.0 mmol) were added in a mixture of 2-ethoxyethanol and water (15−20 mL, v/v = 3:1). The mixture was heated to 80−90 °C and stirred for 16 h. Then the reaction mixture was cooled to room temperature, and water was added. The precipitate of μ-chloro-bridged dimer was collected by filtration and dried under vacuum. Without further purification, the dimer, Na_2CO_3 (5.0 mmol), and acetylacetone (2.5 mmol) were added in 2-ethoxyethanol (15 mL). The mixture was stirred at 90−100 °C under N_2 for 16 h. After the mixture cooled to room temperature, water was added, and a colored precipitate was collected by filtration. The crude product was chromatographed on a silica column with mixture of petroleum ether (PE) bp 60−90 °C and dichloromethane (DCM) to give a pure colored product after drying.

Pt-PVP (V_{PE}/V_{DCM} = 3:2,Yield 12.3%). ^1H NMR (400 MHz, $CDCl_3$): δ (ppm) 8.82 (d, J = 5.6 Hz, 1H), 7.62 (t, J = 7.6 Hz, 1H), 7.56 (d, J = 6.4 Hz, 2H), 7.37−7.26 (m, 3H), 7.13 (d, J = 8.0 Hz, 1H), 6.91 (t, J = 7.2 Hz, 1H), 6.47 (s, 1H), 5.43 (s, 1H), 2.00 (s, 3H), 1.80 (s, 3H); ^{13}C NMR (100 MHz, $CDCl_3$): δ (ppm) 185.31, 184.01, 171.00, 163.90, 146.66, 144.67, 138.34, 130.98, 127.32, 127.27, 126.89, 119.25, 117.78, 102.26, 28.03, 26.93; FAB-MS (m/z): 474 $[M]^+$; Anal.

Calcd for $C_{18}H_{17}NO_2Pt$: C, 45.57; H, 3.61; N, 2.95; found: C, 45.69; H, 3.38; N, 2.60%.

Pt-PVB (V_{PE}/V_{DCM} = 3:2, Yield 19.7%). ^1H NMR (400 MHz, $CDCl_3$): δ (ppm) 8.81 (d, J = 5.6 Hz, 1H), 7.63 (t, J = 8.0 Hz, 1H), 7.49 (dd, J = 11.2 Hz, 4.4 Hz, 4H), 7.13 (d, J = 8.0 Hz, 1H), 6.92 (t, J = 7.6 Hz, 1H), 6.82 (s, 4H), 6.51 (s, 1H), 5.43 (s, 1H), 2.31 (s, 6H, Me), 2.04 (s, 12H, Me), 2.00 (s, 3H), 1.75 (s, 3H); ^{13}C NMR (100 MHz, $CDCl_3$): δ (ppm) 185.30, 183.94, 170.89, 163.77, 148.91, 146.74, 143.80, 142.05, 140.87, 138.37, 138.27, 136.02, 131.59, 128.06, 126.75, 119.43, 118.03, 102.28, 28.01, 26.91, 23.51, 21.22; FAB-MS (m/z): 722 $[M]^+$; Anal. Calcd for $C_{36}H_{38}BNO_2Pt$: C, 59.84; H, 5.30; N, 1.94; found: C, 59.78; H, 5.50; N, 1.90%.

Pt-PVSi (V_{PE}/V_{DCM} = 1:3, Yield 36.3%). ^1H NMR (400 MHz, $CDCl_3$): δ (ppm) 8.81 (d, J = 5.6 Hz, 1H), 7.64−7.56 (m, 9H), 7.48 (d, J = 7.6 Hz, 2H), 7.42−7.35 (m, 9H), 7.13 (d, J = 7.6 Hz, 1H), 6.91 (t, J = 6.0 Hz, 1H), 6.49 (s, 1H), 5.43 (s, 1H), 2.00 (s, 3H), 1.80 (s, 3H); ^{13}C NMR (100 MHz, $CDCl_3$): δ (ppm) 185.35, 183.97, 170.97, 163.67, 146.70, 145.51, 138.37, 136.53, 135.47, 134.46, 134.02, 131.13, 128.98, 128.18, 127.02, 119.35, 117.89, 102.29, 28.05, 26.90; FAB-MS (m/z): 732 $[M]^+$; Anal. Calcd for $C_{36}H_{31}NO_2PtSi$: C, 59.00; H, 4.26; N, 1.91; found: C, 58.89; H, 4.19; N, 1.81%.

Pt-PVGe (V_{PE}/V_{DCM} = 1:3, Yield 35.5%). ^1H NMR (400 MHz, $CDCl_3$): δ (ppm) 8.81 (d, J = 5.2 Hz, 1H), 7.65−7.50 (m, 11H), 7.45−7.34 (m, 9H), 7.14 (d, J = 8.0 Hz, 1H), 6.92 (t, J = 7.6 Hz, 1H), 6.49 (s, 1H), 5.43 (s, 1H), 2.00 (s, 3H), 1.80 (s, 3H); ^{13}C NMR (100 MHz, $CDCl_3$): δ (ppm) 185.34, 183.96, 170.97, 146.71, 145.98, 138.37, 136.47, 135.52, 134.64, 131.17, 129.45, 127.78, 126.63, 119.37, 117.92, 102.29, 28.05, 26.90; FAB-MS (m/z): 778 $[M]^+$; Anal. Calcd for $C_{36}H_{31}NO_2PtGe$: C, 55.62; H, 4.02; N, 1.80; found: C, 55.59; H, 4.19; N, 1.69%.

Pt-PVN (V_{PE}/V_{DCM} = 1:5, Yield 18.7%). ^1H NMR (400 MHz, $CDCl_3$): δ (ppm) 8.80 (d, J = 5.6 Hz, 1H), 7.59 (t, J = 8.0 Hz, 1H), 7.49 (d, J = 8.8 Hz, 2H), 7.25−7.22 (m, 5H), 7.14−7.10 (m, 4H), 7.04−6.97 (m, 4H), 6.87 (t, J = 6.0 Hz, 1H), 6.47 (s, 1H), 5.44 (s, 1H), 2.00 (s, 3H), 1.83 (s, 3H); ^{13}C NMR (100 MHz, $CDCl_3$): δ (ppm) 185.39, 183.86, 171.13, 163.15, 148.01, 147.89, 146.79, 146.61, 139.22, 138.23, 129.94, 129.11, 128.36, 124.21, 124.05, 123.90, 123.57, 122.93, 122.52, 122.35, 122.28, 119.05, 117.41, 102.27, 28.06, 26.92; FAB-MS (m/z): 641 $[M]^+$; Anal. Calcd for $C_{30}H_{26}N_2O_2Pt$: C, 56.16; H, 4.08; N, 4.37; found: C, 56.20; H, 4.10; N, 4.28%.

Pt-PVPO (V_{PE}/V_{DCM} = 1:5, Yield 17.9%). ^1H NMR (400 MHz, $CDCl_3$): δ (ppm) 8.82 (d, J = 5.2 Hz, 1H), 7.71−7.43 (m,15H), 7.15 (d, J = 8.0 Hz, 1H), 6.95 (t, J = 8.8 Hz, 1H), 6.50 (s, 1H), 5.44 (s, 1H), 2.00 (s, 3H), 1.77 (s, 3H); ^{13}C NMR (100 MHz, $CDCl_3$): δ (ppm) 185.47, 183.94, 170.61, 162.05, 148.66, 146.77, 138.52, 133.53, 132.49, 132.20, 132.10, 131.78, 131.75, 131.29, 131.19, 130.24, 129.18, 128.46, 128.34, 127.31, 127.18, 119.64, 118.36, 102.37, 28.01, 26.92; ^{31}P NMR (161.9 MHz, $CDCl_3$): δ (ppm) 29.63; FAB-MS (m/z): 674 $[M]^+$; Anal. Calcd for $C_{30}H_{26}NO_3PPt$: C, 53.41; H, 3.88; N, 2.08; found: C, 53.27; H, 4.10; N, 1.98%.

Pt-PVO (V_{PE}/V_{DCM} = 1:5, Yield 14.5%). ^1H NMR (400 MHz, $CDCl_3$): δ (ppm) 8.81 (d, J = 5.6 Hz, 1H), 7.62 (t, J = 8.0 Hz, 1H), 7.56 (d, J = 8.4 Hz, 2H), 7.36−7.31 (m, 3H), 7.14−7.02 (m, 4H), 6.96 (d, J = 8.8 Hz, 1H), 6.91 (t, J = 6.0 Hz, 1H), 6.47 (s, 1H), 5.44 (s, 1H), 2.00 (s, 3H), 1.83 (s, 3H); ^{13}C NMR (100 MHz, $CDCl_3$): δ (ppm) 185.42, 183.95, 156.26, 146.63, 138.31, 130.44, 129.63, 128.79, 127.30, 122.92, 119.15, 118.72, 117.87, 117.64, 102.29, 28.03, 26.91; FAB-MS (m/z): 566 $[M]^+$; Anal. Calcd for $C_{24}H_{21}NO_3Pt$: C, 50.88; H, 3.74; N, 2.47; found: C, 50.56; H, 3.58; N, 2.29%.

Pt-PVS (V_{PE}/V_{DCM} = 1:3,Yield 37.8%). ^1H NMR (400 MHz, $CDCl_3$): δ (ppm) 8.81 (d, J = 5.6 Hz, 1H), 7.62 (t, J = 8.0 Hz, 1H), 7.53 (d, J = 8.0 Hz, 2H), 7.34−7.18 (m, 7H), 7.12 (d, J = 8.0 Hz, 1H), 6.91 (t, J = 6.4 Hz, 1H), 6.48 (s, 1H), 5.44 (s, 1H), 2.00 (s, 3H), 1.80 (s, 3H); ^{13}C NMR (100 MHz, $CDCl_3$): δ (ppm) 185.41, 183.92, 170.83, 162.62, 146.68, 144.06, 138.37, 136.91, 133.03, 131.08, 130.85, 130.06, 129.00, 128.17, 126.44, 119.34, 117.92, 102.29, 28.01, 26.91; FAB-MS (m/z): 582 $[M]^+$; Anal. Calcd for $C_{24}H_{21}NO_2PtS$: C, 49.48; H, 3.63; N, 2.40; found: C, 49.35; H, 3.59; N, 2.23%.

Pt-PVSO$_2$ (V_{PE}/V_{DCM} = 0:1, Yield 37.5%). ^1H NMR (400 MHz, $CDCl_3$): δ (ppm) 8.82 (d, J = 5.6 Hz, 1H), 7.96−7.94 (m, 2H), 7.86 (d, J = 8.4 Hz, 2H), 7.65−7.62 (m, 3H), 7.54−7.46 (m, 3H), 7.14 (d, J = 7.6 Hz, 1H), 6.91 (t, J = 6.0 Hz, 1H), 6.47 (s, 1H), 5.43 (s, 1H), 2.00 (s, 3H), 1.75 (s, 3H); ^{13}C NMR (100 MHz, $CDCl_3$): δ (ppm) 185.55, 183.92, 170.33, 160.77, 150.17, 146.78, 142.22, 138.82, 138.60, 132.86, 132.67, 129.14, 127.99, 127.50, 126.82, 119.82, 118.64, 102.40, 27.98, 26.89; FAB-MS (m/z): 614 $[M]^+$; Anal. Calcd for $C_{24}H_{21}NO_4PtS$: C, 46.90; H, 3.44; N, 2.28; found: C, 46.79; H, 3.19; N, 2.13%.

OLED Fabrication and Measurements. The precleaned indium tin oxide (ITO) glass substrates were treated with ozone for 20 min. Then, the PEDOT:PSS was deposited on the surface of ITO glass by spin-coating method to form a 45 nm thick hole-injection layer after being cured at 120 °C for 30 min in the air. The emission layer (30 nm) was obtained by spin-coating a chloroform solution of each phosphorescent dopant (x wt %) in TCTA at various concentrations. The obtained ITO chip was dried in a vacuum oven at 60 °C for 10 min and it was transferred to the deposition system for organic and metal deposition. TPBi (45 nm), LiF (1 nm), and Al cathode (100 nm) were successively evaporated at a base pressure less than 10^{-6} Torr. The EL spectra and CIE coordinates were measured with a PR650 spectra colorimeter. The $L-V-J$ curves of the devices were recorded by a Keithley 2400/2000 source meter, and the luminance was measured using a PR650 SpectraScan spectromter. All the experiments and measurements were carried out under ambient conditions.

■ ASSOCIATED CONTENT

Ⓢ Supporting Information

Crystallographic data are given in CIF format. Crystal-packing diagrams of Pt-PVB, Pt-PVSO$_2$, Pt-PVS, Pt-PVSi, and Pt-PVGe and the concerned EL results for all the devices. This material is available free of charge via the Internet at http://pubs.acs.org.

■ AUTHOR INFORMATION

Corresponding Authors

*E-mail: zhougj@mail.xjtu.edu.cn. Fax: (+86)29-82663914. (G.Z.)

*E-mail: ddwang@mail.xjtu.edu.cn. (D.W.)

Notes

The authors declare no competing financial interest.

■ ACKNOWLEDGMENTS

This work was financially supported by Tengfei Project from Xi'an Jiaotong University, the Fundamental Research Funds for the Central Universities, The Program for New Century Excellent Talents in University, the Ministry of Education of China (NECT-09-0651), the Key Creative Scientific Research Team in Shaanxi Province (2013KCT-05), the China Postdoctoral Science Foundation (Grant No. 20130201110034), and the National Natural Science Foundation of China (No. 20902072).

■ REFERENCES

(1) Baldo, M. A.; O'Brien, D. F.; You, Y.; Shoustikov, A.; Sibley, S.; Thompson, M. E.; Forrest, S. R. *Nature* **1998**, *395*, 151−154.

(2) Williams, J. A. G.; Develay, S.; Rochester, D. L.; Murphy, L. *Coord. Chem. Rev.* **2008**, *252*, 2596−2611.

(3) Wang, Z.; Helander, M.; Hudson, Z.; Qiu, J.; Wang, S.; Lu, Z. *Appl. Phys. Lett.* **2011**, *98*, 213301.

(4) Fukagawa, H.; Shimizu, T.; Hanashima, H.; Osada, Y.; Suzuki, M.; Fujikake, H. *Adv. Mater.* **2012**, *24*, 5099−5103.

(5) (a) Yang, X. L.; Yao, C. L.; Zhou, G. J. *Platinum Met. Rev.* **2013**, *57*, 2−16. (b) Wong, W.-Y.; Ho, C.-L. *Coord. Chem. Rev.* **2009**, *253*, 1709−1758. (c) Zhou, G. J.; Wong, W. Y.; Yang, X. L. *Chem.—Asian J.* **2011**, *6*, 1706−1727. (d) Wong, W.-Y.; Ho, C.-L. *J. Mater. Chem.* **2009**, *19*, 4457−4482.

(6) Shao, Y.; Yang, Y. *Adv. Mater.* **2005**, *17*, 2841−2844.

(7) Kim, I.; Haverinen, H. M.; Wang, Z.; Madakuni, S.; Kim, Y.; Li, J.; Jabbour, G. E. *Chem. Mater.* **2009**, *21*, 4256−4260.
(8) (a) Perez, M. D.; Borek, C.; Djurovich, P. I.; Mayo, E. I.; Lunt, R. R.; Forrest, S. R.; Thompson, M. E. *Adv. Mater.* **2009**, *21*, 1517−1520. (b) Wong, W.-Y.; Ho, C.-L. *Acc. Chem. Res.* **2010**, *43*, 1246−1256. (c) Wong, W.-Y.; Wang, X.-Z.; He, Z.; Djurisic, A. B.; Yip, C.-T.; Cheung, K.-Y.; Wang, H.; Mak, C. S. K.; Chan, W.-K. *Nat. Mater.* **2007**, *6*, 521−527. (d) Liu, L.; Ho, C.-L.; Wong, W.-Y.; Cheung, K.-Y.; Fung, M.-K.; Lam, W.-T.; Djurišić, A. B.; Chan, W.-K. *Adv. Funct. Mater.* **2008**, *18*, 2824−2833. (e) Wong, W.-Y.; Wang, X.-Z.; He, Z.; Chan, K.-K.; Djurišić, A. B.; Cheung, K.-Y.; Yip, C.-T.; Ng, A. M.-C.; Xi, Y. Y.; Mak, C. S. K.; Chan, W.-K. *J. Am. Chem. Soc.* **2007**, *129*, 14372−14380. (f) Dai, F.-R.; Zhan, H.-M.; Liu, Q.; Fu, Y.-Y.; Li, J.-H.; Wang, Q.-W.; Xie, Z.; Wang, L.; Yan, F.; Wong, W.-Y. *Chem.—Eur. J.* **2012**, *18*, 1502−1511.
(9) Low, K. H.; Xu, Z. X.; Xiang, H. F.; Chui, S. S. Y.; Roy, V.; Che, C. M. *Chem.—Asian J.* **2011**, *6*, 3223−3229.
(10) Guo, F.; Sun, W.; Liu, Y.; Schanze, K. *Inorg. Chem.* **2005**, *44*, 4055−4065.
(11) Sun, W.; Zhu, H.; Barron, P. M. *Chem. Mater.* **2006**, *18*, 2602−2610.
(12) Zhou, G.; Wong, W. Y.; Poon, S. Y.; Ye, C.; Lin, Z. *Adv. Funct. Mater.* **2009**, *19*, 531−544.
(13) Zhou, G.-J.; Wong, W.-Y. *Chem. Soc. Rev.* **2011**, *40*, 2541−2566.
(14) Peyratout, C. S.; Aldridge, T. K.; Crites, D. K.; McMillin, D. R. *Inorg. Chem.* **1995**, *34*, 4484−4489.
(15) Li, K.; Chen, Y.; Lu, W.; Zhu, N.; Che, C.-M. *Chem.—Eur. J.* **2011**, *17*, 4109−4112.
(16) Yang, X. L.; Huang, Z.; Dang, J. S.; Ho, C. L.; Zhou, G. J.; Wong, W. Y. *Chem. Commun.* **2013**, *49*, 4406−4408.
(17) Adachi, C.; Baldo, M. A.; Forrest, S. R.; Lamansky, S.; Thompson, M. E.; Kwong, R. C. *Appl. Phys. Lett.* **2001**, *78*, 1622−1624.
(18) Brooks, J.; Babayan, Y.; Lamansky, S.; Djurovich, P. I.; Tsyba, I.; Bau, R.; Thompson, M. E. *Inorg. Chem.* **2002**, *41*, 3055−3066.
(19) (a) Baldo, M. A.; Thompson, M. E.; Forrest, S. R. *Pure Appl. Chem.* **1999**, *71*, 2095−2106. (b) Zhou, G.-J.; Wong, W.-Y.; Yao, B.; Xie, Z.; Wang, L. *J. Mater. Chem.* **2008**, *18*, 1799−1809.
(20) Douglas, P.; Eaton, K. *Sens. Actuators, B* **2002**, *82*, 200−208.
(21) O'Donovan, C.; Hynes, J.; Yashunski, D.; Papkovsky, D. B. *J. Mater. Chem.* **2005**, *15*, 2946−2951.
(22) Montes, V. A.; Pérez-Bolívar, C.; Agarwal, N.; Shinar, J.; Anzenbacher, P. *J. Am. Chem. Soc.* **2006**, *128*, 12436−12438.
(23) Graham, K. R.; Yang, Y.; Sommer, J. R.; Shelton, A. H.; Schanze, K. S.; Xue, J.; Reynolds, J. R. *Chem. Mater.* **2011**, *23*, 5305−5312.
(24) Adamovich, V.; Brooks, J.; Tamayo, A.; Alexander, A. M.; Djurovich, P. I.; D'Andrade, B. W.; Adachi, C.; Forrest, S. R.; Thompson, M. E. *New J. Chem.* **2002**, *26*, 1171−1178.
(25) (a) Zhou, G.; Wang, Q.; Wang, X.; Ho, C.-L.; Wong, W.-Y.; Ma, D.; Wang, L.; Lin, Z. *J. Mater. Chem.* **2010**, *20*, 7472−7484. (b) Zhou, G.; Wang, Q.; Ho, C.-L.; Wong, W.-Y.; Ma, D.; Wang, L. *Chem. Commun.* **2009**, 3574−3576.
(26) Chen, Y.; Li, K.; Lu, W.; Chui, S. S. Y.; Ma, C. W.; Che, C. M. *Angew. Chem., Int. Ed.* **2009**, *48*, 9909−9913.
(27) Kui, S. C.; Hung, F. F.; Lai, S. L.; Yuen, M. Y.; Kwok, C. C.; Low, K. H.; Chui, S. S. Y.; Che, C. M. *Chem.—Eur. J.* **2012**, *18*, 96−109.
(28) Lu, W.; Mi, B.-X.; Chan, M. C.; Hui, Z.; Che, C.-M.; Zhu, N.; Lee, S.-T. *J. Am. Chem. Soc.* **2004**, *126*, 4958−4971.
(29) Ravindranathan, D.; Vezzu, D. A.; Bartolotti, L.; Boyle, P. D.; Huo, S. *Inorg. Chem.* **2010**, *49*, 8922−8928.
(30) Chang, S.-Y.; Kavitha, J.; Li, S.-W.; Hsu, C.-S.; Chi, Y.; Yeh, Y.-S.; Chou, P.-T.; Lee, G.-H.; Carty, A. J.; Tao, Y.-T. *Inorg. Chem.* **2006**, *45*, 137−146.
(31) Chang, S.-Y.; Chen, J.-L.; Chi, Y.; Cheng, Y.-M.; Lee, G.-H.; Jiang, C.-M.; Chou, P.-T. *Inorg. Chem.* **2007**, *46*, 11202−11212.
(32) (a) Zhou, G. J.; Ho, C. L.; Wong, W. Y.; Wang, Q.; Ma, D. G.; Wang, L. X.; Lin, Z. Y.; Marder, T. B.; Beeby, A. *Adv. Funct. Mater.* **2008**, *18*, 499−511. (b) Zhou, G. J.; Wang, Q.; Ho, C. L.; Wong, W. Y.; Ma, D. G.; Wang, L. X.; Lin, Z. Y. *Chem.—Asian J.* **2008**, *3*, 1830−1841.
(33) Chi, Y.; Chou, P. T. *Chem. Soc. Rev.* **2010**, *39*, 638−655.
(34) Paulose, B. M. J. S.; Rayabarapu, D. K.; Duan, J. P.; Cheng, C. H. *Adv. Mater.* **2004**, *16*, 2003−2007.
(35) Rayabarapu, D. K.; Paulose, B. M. J. S.; Duan, J. P.; Cheng, C. H. *Adv. Mater.* **2005**, *17*, 349−353.
(36) Heck, R.; Nolley, J., Jr. *J. Org. Chem.* **1972**, *37*, 2320−2322.
(37) Rao, Y. L.; Schoenmakers, D.; Chang, Y. L.; Lu, J. S.; Lu, Z. H.; Kang, Y.; Wang, S. *Chem.—Eur. J.* **2012**, *18*, 11306−11316.
(38) Mou, X.; Wu, Y.; Liu, S.; Shi, M.; Liu, X.; Wang, C.; Sun, S.; Zhao, Q.; Zhou, X.; Huang, W. *J. Mater. Chem.* **2011**, *21*, 13951−13962.
(39) Giordano, T.; Rasmussen, P. G. *Inorg. Chem.* **1975**, *14*, 1628−1634.
(40) Velusamy, M.; Chen, C.-H.; Wen, Y. S.; Lin, J. T.; Lin, C.-C.; Lai, C.-H.; Chou, P.-T. *Organometallics* **2010**, *29*, 3912−3921.
(41) (a) Balashev, K. P.; Puzyk, M. V.; Kotlyar, V. S.; Kulikova, M. V. *Coord. Chem. Rev.* **1997**, *159*, 109−120. (b) Kvam, P. I.; Puzyk, M. V.; Balashev, K. P.; Songstad, J. *Acta Chem. Scand.* **1995**, *49*, 335−343.
(42) Verma, S.; Kar, P.; Das, A.; Ghosh, H. N. *Dalton Trans.* **2011**, *40*, 9765−9773.
(43) (a) Tsuboyama, A.; Iwawaki, H.; Furugori, M.; Mukaide, T.; Kamatani, J.; Igawa, S.; Moriyama, T.; Miura, S.; Takiguchi, T.; Okada, S. *J. Am. Chem. Soc.* **2003**, *125*, 12971−12979. (b) Lamansky, S.; Djurovich, P.; Murphy, D.; Abdel-Razzaq, F.; Lee, H.-E.; Adachi, C.; Burrows, P. E.; Forrest, S. R.; Thompson, M. E. *J. Am. Chem. Soc.* **2001**, *123*, 4304−4312.
(44) (a) Ji, Z.; Li, S.; Li, Y.; Sun, W. *Inorg. Chem.* **2010**, *49*, 1337−1346. (b) Zhou, G.-J.; Wang, X.-Z.; Wong, W.-Y.; Yu, X.-M.; Kwok, H.-S.; Lin, Z. *J. Organomet. Chem.* **2007**, *692*, 3461−3473. (c) Monkman, A.; Burrows, H.; Hartwell, L.; Horsburgh, L.; Hamblett, I.; Navaratnam, S. *Phys. Rev. Lett.* **2001**, *86*, 1358.
(45) Murphy, C. B.; Zhang, Y.; Troxler, T.; Ferry, V.; Martin, J. J.; Jones, W. E. *J. Phys. Chem. B* **2004**, *108*, 1537−1543.
(46) (a) Okada, S.; Okinaka, K.; Iwawaki, H.; Furugori, M.; Hashimoto, M.; Mukaide, T.; Kamatani, J.; Igawa, S.; Tsuboyama, A.; Takiguchi, T.; Ueno, K. *Dalton Trans.* **2005**, 1583−1590. (b) Yersin, H. *Highly efficient OLEDs with phosphorescent materials;* John Wiley & Sons: New York, 2008.
(47) Chen, C. T. *Chem. Mater.* **2004**, *16*, 4389−4400.
(48) (a) Xiang, H. F.; Xu, Z. X.; Roy, V. A. L.; Yan, B. P.; Chan, S. C.; Che, C. M.; Lai, P. T. *Appl. Phys. Lett.* **2008**, *92*, 163305. (b) Ho, C. L.; Li, H.; Wong, W. Y. *J. Organomet. Chem.* **2014**, *751*, 261−285. (c) Graham, K. R.; Yang, Y. X.; Sommer, J. R.; Shelton, A. H.; Schanze, K. S.; Xue, J. G.; Reynolds, J. R. *Chem. Mater.* **2011**, *23*, 5305−5312.
(49) (a) You, Y.; An, C. G.; Kim, J. J.; Park, S. Y. *J. Org. Chem.* **2007**, *72*, 6241−6246. (b) Chen, L. Q.; You, H.; Yang, C. L.; Zhang, X. W.; Qin, J. G.; Ma, D. G. *J. Mater. Chem.* **2006**, *16*, 3332−3339. (c) Bae, H. J.; Chung, J.; Kim, H.; Park, J.; Lee, K. M.; Koh, T. W.; Lee, Y. S.; Yoo, S.; Do, Y.; Lee, M. H. *Inorg. Chem.* **2014**, *53*, 128−138. (d) Liu, Z. W.; Guan, M.; Bian, Z. Q.; Nie, D. B.; Gong, Z. L.; Li, Z. B.; Huang, C. H. *Adv. Funct. Mater.* **2006**, *16*, 1441−1448. (e) Song, M.; Park, J. S.; Gal, Y. S.; Kang, S.; Lee, J. Y.; Lee, J. W.; Jin, S. H. *J. Phys. Chem. C* **2012**, *116*, 7526−7533. (f) Ding, J. Q.; Lu, J. H.; Cheng, Y. X.; Xie, Z. Y.; Wang, L. X.; Jing, X. B.; Wang, F. S. *Adv. Funct. Mater.* **2008**, *18*, 2754−2762.
(50) (a) Tung, Y. L.; Chen, L. S.; Chi, Y.; Chou, P. T.; Cheng, Y. M.; Li, E. Y.; Lee, G. H.; Shu, C. F.; Wu, T. I.; Carty, A. J. *Adv. Funct. Mater.* **2006**, *16*, 1615−1626. (b) Tung, Y. L.; Lee, S. W.; Chi, Y.; Chen, L. S.; Shu, C. F.; Wu, F. I.; Carty, A. J.; Chou, P. T.; Peng, S. M.; Lee, G. H. *Adv. Mater.* **2005**, *17*, 1059−1064.
(51) King, K.; Spellane, P.; Watts, R. J. *J. Am. Chem. Soc.* **1985**, *107*, 1431−1432.
(52) Sheldrick, G. M. *SHELXL-97,* Program for Crystal Structure Refinement; University of Göttingen: Göttingen, Germany, 1997.
(53) Sheldrick, G. M. *SADABS;* University of Göttingen: Göttingen, Germany, 1996.
(54) Wadt, W. R.; Hay, P. J. *J. Chem. Phys.* **1985**, *82*, 284−298.

(55) Hay, P. J.; Wadt, W. R. *J. Chem. Phys.* **1985**, *82*, 299−310.
(56) Frisch, M. J.; Trucks, G. W.; Schlegel, H. B.; Scuseria, G. E.; Robb, M. A.; Cheeseman, J. R.; Scalmani, G.; Barone, V.; Mennucci, B.; Petersson, G. A.; Nakatsuji, H.; Caricato, M.; Li, X.; Hratchian, H. P.; Izmaylov, A. F.; Bloino, J.; Zheng, G.; Sonnenberg, J. L.; Hada, M.; Ehara, M.; Toyota, K.; Fukuda, R.; Hasegawa, J.; Ishida, M.; Nakajima, T.; Honda, Y.; Kitao, O.; Nakai, H.; Vreven, T.; Montgomery, J. A., Jr.; Peralta, J. E.; Ogliaro, F.; Bearpark, M.; Heyd, J. J.; Brothers, E.; Kudin, K. N.; Staroverov, V. N.; Kobayashi, R.; Normand, J.; Raghavachari, K.; Rendell, A.; Burant, J. C.; Iyengar, S. S.; Tomasi, J.; Cossi, M.; Rega, N.; Millam, J. M.; Klene, M.; Knox, J. E.; Cross, J. B.; Bakken, V.; Adamo, C.; Jaramillo, J.; Gomperts, R.; Stratmann, R. E.; Yazyev, O.; Austin, A. J.; Cammi, R.; Pomelli, C.; Ochterski, J. W.; Martin, R. L.; Morokuma, K.; Zakrzewski, V. G.; Voth, G. A.; Salvador, P.; Dannenberg, J. J.; Dapprich, S.; Daniels, A. D.; Farkas, O.; Foresman, J. B.; Ortiz, J. V.; Cioslowski, J.; Fox, D. J. *Gaussian 09, Revision A.01;* Gaussian, Inc.: Wallingford, CT, 2009.
(57) Kim, M.; Kwak, J.; Chang, S. *Angew. Chem., Int. Ed.* **2009**, *48*, 8935−8939.